The propagation of weak shocks in non-uniform flows

By N. K.-R. KEVLAHAN†

Department of Applied Mathematics and Theoretical Physics, University of Cambridge,
Silver Street, Cambridge, CB3 9EW, UK

A new theory of the propagation of weak shocks into non-uniform, two-dimensional flows is introduced. The theory is based on a description of shock propagation in terms of a manifold equation together with compatibility conditions for shock strength and its normal derivatives behind the shock. This approach was developed by Ravindran & Prasad (1993) for shocks of arbitrary strength propagating into a medium at rest and is extended here to non-uniform media and restricted to moderately weak shocks. The theory is tested against known analytical solutions for cylindrical and plane shocks, and against a full direct numerical simulation (DNS) of a shock propagating into a sinusoidal shear flow. The test against DNS shows that the present theory accurately predicts the evolution of a moderately weak shock front, including the formation of shock-shocks due to shock focusing. The theory is then applied to the focusing of an initially parabolic shock, and to the propagation of an initially straight shock into a variety of simple flows (sinusoidal shear, vortex array, point-vortex array) exhibiting some fundamental properties of turbulent flows. A number of relations are deduced for the variation of shock quantities with initial shock strength M_{S0} and the Mach number of the flow ahead of the shock M_U (e.g. separation of shock-shocks and maximum shock strength at a focus). It is found that shock-shocks are likely to form in turbulent flows with $M_t/M_{1N} > 0.14$–0.25, where M_t is the average Mach number of the turbulence and M_{1N} is the Mach number of the shock in a flow at rest. The shock moves up to 1.5% faster in a two-dimensional vortex array than in uniform flow.

1. Introduction

1.1. *A review of shock theory*

Theories of shock propagation in more than one dimension may be divided roughly into two groups: the first deals with the propagation (generally in two dimensions) of curved shocks into uniform flows and the second treats the propagation of shocks through non-uniform (e.g. turbulent) flows. The first class of theories includes *weak shock theory* (e.g. Whitham 1974, Chap. 9) and *shock dynamics* (e.g. Whitham 1974, Chap. 8), while the second class includes methods for dealing with the shock–turbulence interaction such as the *linear interaction analysis* (e.g. McKenzie & Westphal 1967) and *rapid distortion theory* (e.g. Lee, Lele & Moin 1993). These two classes of theories treat different limits of the shock propagation problem. The first class is not useful for turbulent flows, but allows the shock to evolve dynamically; the

† Present address: LMD-CNRS, 24, rue Lhomond, 75231 Paris cédex 05, France.

second class is used for turbulent flows, but does not take into account any nonlinear shock evolution. All these theories are approximate, and their domain of accuracy is often difficult to assess *a priori*. A brief description of these theories follows.

Weak shock theory applies to the propagation of very weak shocks and is mainly concerned with the flow profile behind the shock front (the shock wave). In this theory an initial pressure pulse is allowed to propagate along the straight rays given by geometrical acoustics (Keller 1954). The pulse is nonlinearized by allowing the speed of propagation to increase with overpressure. Eventually the shock overturns and at that point shocks are fitted into the pressure profile using the equal-area rule. For weak shocks, the propagation speed of the shock front is proportional to the pressure jump (overpressure at the discontinuity). Thus, the geometry of the shock front is given by geometrical acoustics, and the variation in propagation speed of different parts of the shock wave with overpressure is found from nonlinear aging in ray tubes (Whitham 1974, Chap. 9). Note that the shocks are just fitted in, the propagation of the shock-containing pulse is treated identically to the propagation of the smooth pulse. In this sense, the weak shock is assumed to propagate in the same way as a nonlinear pressure wave.

In the weak shock limit the shock strength is proportional to the inverse of the square root of the ray tube area. If the shock does focus, or form a caustic, the ray tube area vanishes and thus weak shock theory predicts an artificial singularity in the shock strength. Experimentally, the shock strength always remains finite and the shape of the weak shock at the focus does not correspond to that predicted by geometrical acoustics (Sturtevant & Kulkarny 1976). This unphysical behaviour shows that weak shock theory is a poor approximation near a focus.

Obermeier (1983) attempted to remedy weak shock theory near a focus. He suggested transforming the linear waveform just ahead of the focus to a nonlinear waveform by shearing and fitting shocks according to the equal-area rule. The solution is limited to weakly curved converging shock waves of moderately weak strength. This theory is not completely satisfactory since no justification is given for the shearing construction (except weak shock theory, which is invalid at a focus) and there is no 1:1 correspondence between waveforms before and after the focus.

Shock dynamics (Whitham 1957) is a theory which describes the propagation of a strong shock into a flow at rest. In this theory the flow behind the shock is ignored and the shock is treated purely as a propagating discontinuity. Instead of the linear rays of geometrical acoustics, shock dynamics is based on a perpendicular coordinate system made up of shock 'rays' (defined as the orthogonal trajectories of successive points on the shock front) and the successive positions of the shock front itself. The basic idea of the theory is to treat the propagation of each element of the shock down each elementary ray tube in the same way as the propagation of a shock wave down a pipe with solid walls. Because the shock velocity depends on its strength, the ray geometry cannot be mapped out in advance as it can in weak shock theory. The geometry and shock strength are coupled. Shock dynamics has been verified for, among other cases, the diffraction of a shock wave around a circular cylinder (Bryson & Gross 1961).

Shock dynamics has been extended to shocks propagating into flows of uniform motion (Whitham 1968), and to non-uniform media where the non-uniformity is due to the inhomogeneity of the medium, not its motion (Kulkarny & White 1982; Catherasoo & Sturtevant 1983). None of these applications of shock dynamics corresponds to the case of a weak shock interacting with homogeneous, incompressible turbulence considered here.

Neither shock dynamics nor weak shock theory are deduced rigorously as approximations to the exact equations governing shock motion. They are based on reasonable physical assumptions, and their validity has been assessed by applying them to a variety of test flows. As Whitham himself notes (Whitham 1974, p. 264),

> In both cases, the approximations become intuitive and are based on incorporating known effects into a mathematical description. The "justification" comes from checks on particular cases that can be handled precisely and from comparison with observations. The problems are too hard for the more routine approximation procedures.

The accuracy of these theories for a particular problem is thus difficult to judge beforehand, as the failure of weak shock theory near a focus shows. Shock dynamics is extremely accurate in the case of imploding shocks, but was shown by Hayes (1968) to be as much as 15% in error for rising shocks in an atmosphere with exponentially varying density. Recently, the validity of some of the basic assumptions of these theories (such as applying the characteristic rule to shock propagation) has also been questioned (Prasad, Ravindran & Sau 1991).

Shock theories that have been applied to the shock–turbulence interaction tend to take a very different point of view from those described above. Instead of carefully modelling the dynamics of shock evolution, the shock–turbulence theories are interested in the statistics of how the shock is affected by the turbulence and how the turbulence is affected by the shock. To simplify the calculation of these statistics shock evolution is neglected.

The most commonly used shock–turbulence theory is the linear interaction analysis (LIA). This theory was introduced by Moore (1953) and Ribner (1953) and has since been developed by McKenzie & Westphal (1968), Anyiwo & Bushnell (1982) and Lee *et al.* (1993). In LIA one considers turbulence perturbations incident on the shock front to be harmonic waves of the form $A' \exp[i(\boldsymbol{k} \cdot \boldsymbol{r} - \omega t)]$, where A' is small. The incident wave may be vortical or acoustic or entropic (the three wave types decouple for weak turbulence, Kovásznay 1953). One then constructs the linearized perturbed Rankine–Hugoniot jump conditions across the shock. A further assumption is required about the form of the distorted shock in order to solve the perturbed jump equations. It is assumed that the shock merely copies the form of the incoming disturbance (i.e. a sine wave), but with an amplitude determined from the Rankine–Hugoniot equations. This further assumption about the shape of the deformed shock closes the perturbed Rankine–Hugoniot equations and allows velocity, pressure and density behind the shock to be calculated. A wave of a single type hitting the the shock from ahead generates all three wave types behind, and the inclination angle and amplitude of each of these waves can be calculated. By assuming a particular spectrum of incoming turbulence waves (primarily vortical in turbulent flows), one can calculate statistics of quantities behind the shock and shock deformation. The net distortion of the shock in a turbulent flow is given by a superposition of a spectrum of individual sinusoidal distortions.

Rapid distortion theory (RDT) has also been applied to the shock–turbulence interaction (Durbin & Zeman 1992). RDT is usually used to calculate the statistical effects of a mean distortion (such as simple shear) on a turbulent flow. The velocity field is split into mean and fluctuating parts and then substituted into the Navier–Stokes equations. Terms nonlinear in fluctuating quantities are neglected and the equations are transformed to Fourier space. The resulting Fourier-transformed equations can be solved exactly for simple distortions, giving the evolution of the turbulence energy spectrum due to the mean distortion. RDT can be applied to the shock–turbulence

interaction by assuming that the shock just applies a rapid compression to the turbulence (e.g. no shock distortion effects are included), and that the effect of this distortion can be calculated using RDT. Note that this method, unlike LIA, does not include any deformation of the shock front itself and thus can give only a rough estimate of the mean change in the turbulence.

The predictions of LIA and RDT for the shock–turbulence interaction have been compared with a DNS of the same flows by Lee et al. (1993). They found that for turbulence Mach numbers less than the shock strength $(M_t^2 < 0.1(M_S^2 - 1))$ the LIA predictions for r.m.s. shock front displacement and inclination angle are in only fair agreement with DNS. The non-monotonic behaviour of turbulent kinetic energy is well predicted by LIA; however it tends to underestimate the deformation of the shock front (by as much as 25%) and became less accurate as M_t increases. The LIA prediction of the amplification of transverse vorticity is close (within 5%), but systematically lower than the DNS results. This underestimation of the vorticity amplification may be due to the fact that LIA neglects all shock focusing effects, and these can lead to greatly enhanced vorticity jumps (Kevlahan 1996). RDT and LIA predictions for reduction in length scales and velocity amplification across the shock agree with DNS for $M_t^2 < 0.1(M_S^2 - 1)$. The shock front is severely distorted for $M_t^2 > 0.1(M_S^2 - 1)$, and both LIA and RDT fail in this parameter range. DNS also shows a systematic forward drift of the shock front at a speed of about 0.7% of the laminar shock speed; this is not predicted by LIA.

The comparison with DNS shows that even in the range $M_t^2 < 0.1(M_S^2 - 1)$ LIA systematically underestimates the distortion of the shock front, and that this may be the reason LIA underestimates vorticity amplification. LIA also fails to predict the observed increase in propagation speed of the shock. These results indicate that a theory of the shock–turbulence interaction incorporating shock evolution would be a significant improvement.

DNS of the shock turbulence–interaction itself suffers from the problem of having to resolve the internal structure of the shock. This greatly increases the computational time and restricts the simulations to relatively small Mach numbers.

Lele (1992) has analysed statistically the shock-jump relations using an RDT assumption and has also found that the shock speed increases in turbulence. He calculates the increase to be roughly 0.4% of laminar shock speed, 40% lower than the increase measured by Lee et al. (1993). The physical interpretation of Lele's result is that turbulent fluctuations increase across the shock, leading to an increase in turbulent normal stress. The increase in turbulent normal stress produces a corresponding decrease in the pressure rise and that means the shock must travel faster to bring about the specified mean compression. Lele does not include the effects of shock focusing, which, as will be shown, also increases shock speed. One may also expect the mean compression in a turbulent flow to actually evolve over time (as the shock front deforms) and this may further alter the propagation speed of the shock.

1.2. Objectives and overview

As seen in the previous subsection, the theories of the propagation of shocks through turbulence (LIA and RDT) do not take into account shock evolution, while theories describing shock evolution (weak shock theory and shock dynamics) are really only useful for uniform flows at rest, or with simple non-uniformities. Furthermore, neither weak shock theory nor shock dynamics are deduced formally as approximations to the exact equations governing shock motion, and therefore their domain of validity is difficult to assess. The comparison with DNS carried out by Lee et al. (1993)

has shown that there is also room for improvement in the LIA theory of the shock–turbulence interaction.

The objectives of this paper are to derive, test and apply a new theory of the interaction of weak shocks with non-uniform flow. This theory should be applicable to turbulence and include shock evolution. It should also be able to predict correctly the behaviour of a weak shock at a focus (unlike weak shock theory). By applying the theory to a variety of simple flows the way a shock alters when encountering non-uniform flows is examined in detail. Specific questions addressed include: What is the maximum shock strength at a focus? How does the separation of shock-shocks at a focus vary with shock strength? When will a shock focus in a non-uniform flow? How is shock speed altered by a non-uniform flow? When does the evolution of the shock become significant, and can any general properties be deduced?

In §2 a new theory of the interaction of a moderately weak shock with a non-uniform flow is introduced. This theory is based on the approach using the shock manifold equation with compatibility conditions of Ravindran & Prasad (1993) who treated the shock as a propagating discontinuity and included the effect of the flow behind the shock through the compatibility conditions on the normal derivatives of shock strength. For simplicity the theory is worked out in two dimensions, although it can in principle be extended to three dimensions. The exact description of Ravindran & Prasad (1993) (which involves an infinite hierarchy of compatibility conditions) is closed by considering only moderately weak shocks. Both first- and second-order approximations in shock strength are derived. The theory is also generalized to the case of non-uniform moving flows with $M_i^2 \ll 1$.

The numerical method used to solve the shock equations is described in §3. In §4 the theory is verified against known analytical solutions in special cases and against a DNS of a shock propagating into a sinusoidal shear flow. The shock focusing problem is examined in detail in §5.1 where the evolution of an initially parabolic shock is calculated. The theory is then applied to a variety of simple flows exhibiting some basic properties of turbulence. These flows are a sinusoidal shear flow (§5.2), a two-dimensional array of vortices (§5.3), and a linear array of point vortices (§5.4). Finally, in §6 the results are summarized and the implications for the shock–turbulence interaction are deduced.

2. A new theory of the propagation of weak shocks in non-uniform flows

2.1. *Assumptions*

We consider the propagation in two dimensions of a shock front in a ideal polytropic gas with a constant ratio of specific heats γ. In principle the theory could be extended to three dimensions. The gasdynamic approximation is made, i.e. viscous and heat conduction effects are omitted and the flow is governed by the compressible Euler equations. The shock front is treated as a discontinuity. The assumption of zero shock thickness is justified if either the minimum radius of curvature of the shock is much greater than the shock thickness, $R_{min} \gg \Delta$, or if a discontinuity which is placed initially within the thickness of the shock front remains there. The validity of this assumption is tested by comparison with a DNS which actually resolves the internal structure of the shock.

The Mach number of the shock $M_s = C_s/a$, where $a = (\gamma P/\rho)^{1/2}$ is the speed of sound, is assumed to be moderately weak, i.e. $1 \leqslant M_s < 1.5$. The upper limit is chosen

because if $M_s < 1.5$, then the normalized jump in density μ (which is the Taylor expansion parameter) is less than one.

The fluid velocity u, pressure P and density ρ are assumed to be smooth functions except for a discontinuity of the first kind (i.e. limits exist from both ahead of and behind the shock) on the shock surface Ω. The state ahead of the shock is allowed to be non-uniform and in motion, but it is assumed that eddy shocklets do not form (which limits the turbulence Mach number, $M_t = (\overline{u'_j u'_j}/a^2)^{1/2} < 0.3$, and means that there must be little kinetic energy in the dilatational mode, Kida & Orszag 1990).

The approximations used for the flow ahead are the following. Let normalized non-uniform quantities be denoted by a tilde and stagnation quantities (the value in a flow at rest) be denoted by the subscript 0, then $\tilde{P} = P/P_0 - 1$, $\tilde{\rho} = \rho/\rho_0 - 1$ and $\tilde{u} = u/a_0$. It is assumed that products of ($\tilde{\ }$) quantities can be neglected (the acoustic approximation).

Making the acoustic approximation, the continuity equation $\partial\rho/\partial t + \nabla \cdot (\rho u) = 0$ becomes

$$\frac{\partial\tilde{\rho}}{\partial t} = -\nabla \cdot \tilde{u}, \tag{2.1}$$

and using the fact that for isentropic flows $\tilde{P} = \gamma\tilde{\rho}$, the Euler equation $\partial u/\partial t + u \cdot \nabla u = -(1/\rho)\nabla P$ becomes

$$\nabla\tilde{\rho} = -\frac{\partial\tilde{u}}{\partial t}, \tag{2.2}$$

where we have normalized length by $1/k$ and time by $1/(a_0 k)$ where k is a characteristic wavenumber of the flow. Relations (2.1) and (2.2), together with the isentropic relation, allow gradients and time derivatives of pressure and density ahead of the shock to be expressed in terms of the velocity ahead of the shock.

If the flow ahead of the shock varies on a time scale τ long compared with $a_0 k$ then the flow is approximately *steady* and the variation in sound speed a is

$$\left(\frac{a}{a_0}\right)^2 = 1 - \tfrac{1}{2}(\gamma - 1)M_U^2 \tag{2.3}$$

where $M_U^2 = \tilde{u} \cdot \tilde{u}$ is the local Mach number. Thus the sound speed of the flow ahead of the shock is constant, $a = a_0$, since M_U^2 is neglected in the acoustic approximation. Since $a^2/a_0^2 \sim 1 + (\gamma - 1)\tilde{\rho}$, this means that the flow is incompressible to $O(M_U)$ and the flow ahead of the shock generates no free-stream acoustic perturbations.

The shock strength is represented by the normalized density jump, or condensation μ

$$\mu = \frac{\rho_b - \rho_a}{\rho_a}, \tag{2.4}$$

and it is assumed that the shock is *weak*, i.e.

$$\mu \ll 1 \tag{2.5}$$

(μ is less than 1 to $O(\mu)$ provided $M_s < 1.5$). Tangential derivatives of shock strength along the shock are also assumed to be small, i.e. $\partial\mu/\partial S = O(\mu)$, but normal derivatives of shock strength may be of order 1, i.e. $\partial\mu/\partial N = O(1)$. Because $\partial\mu/\partial S$ is assumed small, the theory is invalid if the shock surface does not remain smooth (e.g. when the shock develops kinks at a focus).

As stated above, the acoustic approximation is used for the flow ahead of the shock and terms nonlinear in these quantities are neglected. We retain, however,

terms involving products of μ and fluctuating quantities ahead of the shock. Since nonlinear upstream terms only appear multiplied by μ in the shock equations it must be assumed that

$$M_U^2 \mu \leqslant O(\mu^2), \tag{2.6}$$

or

$$M_U^2 \leqslant O(\mu), \tag{2.7}$$

where M_U^2 is taken as an estimate of the magnitude of products of quantities ahead of the shock. Combining conditions (2.5) and (2.7) the range of validity of the shock propagation theory derived in the following section is

$$M_U^2 \leqslant \mu \ll 1. \tag{2.8}$$

To first order in μ the range (2.8) may be expressed in terms of M_s as

$$\tfrac{1}{4}(\gamma + 1)M_U^2 \leqslant M_s - 1 \ll 1. \tag{2.9}$$

For $\gamma = 1.4$, $(\gamma + 1)/4 = 0.6$.

2.2. *Derivation of the first-order approximation*

In this section we describe shock propagation in terms of compatibility conditions on a shock manifold in space–time. This method was first proposed by Grinfel'd (1978) and Maslov (1978) and has since been developed for arbitrary shock strength and uniform flows ahead of the shock by Ravindran & Prasad (1993). The shock manifold equation describes how the shape of the shock evolves. The compatibility conditions describe the evolution of normal derivatives of a single variable (such as μ) behind the shock and are in the form of transport equations along shock rays (defined by the successive positions of points on the shock). The effect of the flow behind the shock is represented by these compatibility conditions. In general, an infinite number of compatibility conditions is required (i.e. normal derivatives of μ of all orders) and the system of equations governing shock propagation is not closed. Requiring an infinite number of compatibility conditions is equivalent to saying that the *entire* flow behind affects the shock. As we shall see below, for weak shocks only the first two compatibility conditions are required. The theory of Ravindran & Prasad (1993) is closed here by the restriction to weak shocks and is extended to non-uniform flows ahead of the shock.

Consider a discontinuous shock Ω dividing the flow into two domains which we will denote by the subscripts a (the region ahead of the shock) and b (the region behind the shock), see figure 1. The shock motion is calculated in a frame of reference in which the mean velocity of the flow ahead is zero. The functions to the left u_b, P_b and ρ_b are defined only in the domain behind the shock, but are extended as C^∞ functions on the whole of $\Re^2$. The extended functions are non-unique in the domain ahead of the shock. The functions in the right-hand domain are similarly extended into the domain behind the shock. In particular, the shock strength μ is now defined over the whole of $\Re^2$, i.e.

$$\mu = \mu(x, y, t) = \frac{\rho_b(x, y, t) - \rho_a(x, y, t)}{\rho_a(x, y, t)}, \tag{2.10}$$

and the actual shock strength is the value of μ at the shock $\mu(x, y, t)|_\Omega$. The extension of flow quantities behind the shock to the whole domain allows the definition of normal derivatives of μ (and other quantities). These normal derivatives are required
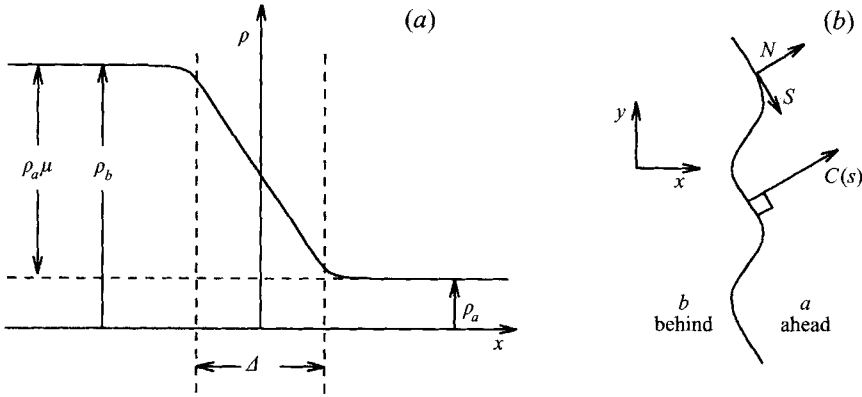
FIGURE 1. Shock properties. (a) Internal structure of a shock. $\mu = (\rho_b - \rho_a)/\rho_a$ is the shock strength and $\Delta = 3A(1 - \frac{1}{2}(\gamma - 1)\mu)^{1/2}/[(1 + \mu)^{1/2} - (1 - \frac{1}{2}(\gamma - 1)\mu)^{1/2}]$ is the shock thickness. (b) Shock geometry in a reference frame in which the mean flow ahead of the shock is zero (this frame is used throughout the paper).

to construct the compatibility equations which describe the effect of the flow behind on the shock.

Hunt & Vassilicos (1991) have shown that turbulence cannot be C^∞ at the length scales of the inertial range (because its inertial-range energy spectrum follows a non-integer power law $E(k) \propto k^{-5/3}$), but, as is shown later, only the first normal derivative $\partial\mu/\partial N$ is required for the first-order shock propagation theory. Thus for weak shocks the flow ahead of the shock need only be C^1, provided the shock is smooth so the neglected normal derivative terms do not become singular.

Let $g(x, y, t) = 0$ denote the equation of the shock surface Ω in space–time. In order that the jump relations for the conservation of mass, momentum and energy across a shock have a non-trivial solution (e.g. a non-zero jump in the flow density) the determinant Δ of the matrix of coefficients of δu, δv, δP and $\delta\rho$ (where δ denotes the jump of a quantity) must be zero. Prasad (1982) was able to show that the condition $\Delta = 0$ implies that the shock surface must satisfy Prandtl's relation in the form

$$\frac{Dg}{Dt} + C_r|\nabla g| = 0 \quad \text{on} \quad g(x, y, t) = 0 \tag{2.11}$$

where C_r is the propagation speed of the shock relative to the flow ahead. Equation (2.11) describes a surface propagating in its normal direction with speed C_r and being advected by the flow ahead of the shock. An embedding theorem (Courant & Hilbert 1953, vol. 2, pp. 557–558) can then be used to obtain a one-parameter family of shocks $G(x, y, t) = $ const., where the function G satisfies the equation (2.11).

The shock manifold equation (SME) describes the evolution of a scalar field $G(x, y, t)$ where the zero-level surface $G = 0$ represents the physical shock front. A similar description was first proposed for the propagation of a flamelet by Williams (1985) and has been used recently by Peters (1992), where it is called a 'field equation' or 'Williams equation'. The application of the simplest field equation model (in which the propagation speed is assumed constant) to the shock–turbulence interaction is described in Kevlahan, Krishnan & Lee (1992).

If the shock does not curl around on itself the scalar field variable $G(x, y, t)$ may be defined as

$$G(x, y, t) = x - g(y, t), \tag{2.12}$$

then the SME on the level surface $G(x, y, t) = 0$ becomes

$$g_t = u_r - v_r g_y + C_r (1 + g_y^2)^{1/2}. \tag{2.13}$$

In general, the propagation speed is a function of time and position, $C_r = C_r(x, y, t)$.

The unit normal and unit tangent vectors to the shock front Ω are, respectively, $N = (N_1, N_2) = (\cos\theta, \sin\theta)$, and $S = (N_2, -N_1) = (\sin\theta, -\cos\theta)$. The SME is valid in $\Re^2$ and it is therefore possible to define the angle θ in $\Re^2$ using the relations

$$N = (N_1, N_2) = \frac{\nabla G}{|\nabla G|} = \frac{(G_x, G_y)}{(G_x^2 + G_y^2)^{1/2}}. \tag{2.14}$$

The equations for the motion of points on the shock surface are given by the characteristic equations of the SME

$$\frac{dX}{dt} = \tilde{u}_r + C_r N_1, \tag{2.15}$$

$$\frac{dY}{dt} = \tilde{v}_r + C_r N_2, \tag{2.16}$$

$$\frac{dG_x}{dt} = -\left(\frac{\partial \tilde{u}_a}{\partial x} G_x + \frac{\partial \tilde{v}_a}{\partial x} G_y + \frac{\partial C_r}{\partial x} (G_x^2 + G_y^2)^{1/2} \right), \tag{2.17}$$

$$\frac{dG_y}{dt} = -\left(\frac{\partial \tilde{u}_a}{\partial y} G_x + \frac{\partial \tilde{v}_a}{\partial y} G_y + \frac{\partial C_r}{\partial y} (G_x^2 + G_y^2)^{1/2} \right), \tag{2.18}$$

and using (2.17) and (2.18) the variation in the shock normal angle θ is

$$\frac{d\theta}{dt} = -\frac{1}{N_2} \frac{dN_1}{dt} + \frac{1}{N_1} \frac{dN_2}{dt} = \frac{\partial C_r}{\partial S} + N_1 \frac{\partial \tilde{u}_a}{\partial S} + N_2 \frac{\partial \tilde{v}_a}{\partial S}. \tag{2.19}$$

Equation (2.19) shows how gradients in shock propagation speed (e.g. due to curvature via equation (2.43)) turn the shock and cause the 'shock-rays' to curve.

The Rankine–Hugoniot jump conditions for the conservation of mass, momentum and energy lead to the following relations on Ω:

$$C|_\Omega = a_0 \left(\frac{1 + \mu}{1 - \frac{1}{2}(\gamma - 1)\mu} \right)^{1/2} \Bigg|_\Omega + A_a|_\Omega, \tag{2.20}$$

$$P_b|_\Omega = \frac{\rho_a \mu C_r^2}{1 + \mu} \Bigg|_\Omega + P_a|_\Omega, \tag{2.21}$$

$$A_b|_\Omega = \frac{\mu C_r}{1 + \mu} \Bigg|_\Omega + A_a|_\Omega, \tag{2.22}$$

$$B_b|_\Omega = B_a|_\Omega, \tag{2.23}$$

where $C_r = C - A_a$ is the propagation speed in an upstream flow at rest (the first term on the left-hand side of (2.20)), and A_a and B_a are the normal and tangential components of the velocity field ahead of the shock

$$A = N \cdot u = N_1 u + N_2 v, \tag{2.24}$$

$$B = S \cdot u = N_2 u - N_1 v, \tag{2.25}$$

For weak shocks, i.e. $\mu \ll 1$, the relations (2.20)–(2.23) reduce to

$$C|_\Omega = a_0 (1 + \frac{1}{4}(\gamma + 1)\mu)|_\Omega + A_a|_\Omega, \tag{2.26}$$

$$P_b|_\Omega = \rho_0 a_0^2 \mu + P_0|_\Omega, \qquad (2.27)$$

$$A_b|_\Omega = a_0 \mu|_\Omega, \qquad (2.28)$$

$$B_b|_\Omega = B_a|_\Omega, \qquad (2.29)$$

where the approximation $\rho_a = \rho_0 + O(M_U^2)$ has been used (from (2.3)).

In the weak shock approximation equations (2.15), (2.16) and (2.19) become respectively

$$\frac{\mathrm{d}X}{\mathrm{d}t} = N_1 \left(1 + \tfrac{1}{4}(\gamma + 1)\mu\right) + \tilde{u}_a, \quad \frac{\mathrm{d}Y}{\mathrm{d}t} = N_2 \left(1 + \tfrac{1}{4}(\gamma + 1)\mu\right) + \tilde{v}_a \qquad (2.30)$$

and

$$\frac{\mathrm{d}\theta}{\mathrm{d}t} = \tfrac{1}{4}(\gamma + 1)\frac{\partial\mu}{\partial S} + N_1 \frac{\partial\tilde{u}_a}{\partial S} + N_2 \frac{\partial\tilde{v}_a}{\partial S}. \qquad (2.31)$$

Note that if $\mu = 0$ we recover the ray equations of geometrical acoustics.

We will now derive the first compatibility equation which describes how μ (and hence C_r) varies in time. The gasdynamics equations for the conservation of mass, momentum and energy are

$$\rho_t + (u,v) \begin{pmatrix} \rho_x \\ \rho_y \end{pmatrix} + \rho(u_x + v_y) = 0, \qquad (2.32)$$

$$\begin{pmatrix} u_t \\ v_t \end{pmatrix} + \begin{pmatrix} u_x & u_y \\ v_x & v_y \end{pmatrix} \begin{pmatrix} u \\ v \end{pmatrix} + \frac{1}{\rho} \begin{pmatrix} P_x \\ P_y \end{pmatrix} = 0, \qquad (2.33)$$

$$P_t + (u,v) \begin{pmatrix} P_x \\ P_y \end{pmatrix} + \gamma P(u_x + v_y) = 0. \qquad (2.34)$$

(Note that the acoustic approximation has not been made yet.)

Following Ravindran & Prasad (1993) these conservation equations may be written in terms of normal and tangential differential operators:

$$\frac{\partial}{\partial N} = \mathbf{N} \cdot \nabla = N_1 \frac{\partial}{\partial x} + N_2 \frac{\partial}{\partial y}, \quad \frac{\partial}{\partial S} = \mathbf{S} \cdot \nabla = N_2 \frac{\partial}{\partial x} - N_1 \frac{\partial}{\partial y}, \qquad (2.35)$$

and the time derivative may be expressed as time rate of change following the shock:

$$\frac{\mathrm{d}}{\mathrm{d}t} = \frac{\partial}{\partial t} + C\frac{\partial}{\partial N}. \qquad (2.36)$$

Remembering that because they contain vector information the normal, tangential and time differential operators do not commute for a function $F(x, y, t)$, i.e.

$$\frac{\partial}{\partial N}\left(\frac{\partial F}{\partial S}\right) = \frac{\partial}{\partial S}\left(\frac{\partial F}{\partial N}\right) + \frac{\partial\theta}{\partial S}\frac{\partial F}{\partial S} + \frac{\partial\theta}{\partial N}\frac{\partial F}{\partial N}, \qquad (2.37)$$

$$\frac{\partial}{\partial N}\left(\frac{\mathrm{d}F}{\mathrm{d}t}\right) = \frac{\mathrm{d}}{\mathrm{d}t}\left(\frac{\partial F}{\partial N}\right) + \frac{\mathrm{d}\theta}{\mathrm{d}t}\frac{\partial F}{\partial S} + \frac{\partial C}{\partial N}\frac{\partial F}{\partial N} - C\frac{\partial\theta}{\partial N}\frac{\partial F}{\partial S}, \qquad (2.38)$$

after some manipulation the conservation equations become

$$\frac{\mathrm{d}\rho}{\mathrm{d}t} + (A - C)\frac{\partial\rho}{\partial N} + \rho\left(\frac{\partial A}{\partial N} - A\frac{\partial\theta}{\partial S}\right) + \left[B\frac{\partial\rho}{\partial S} + \rho\left(\frac{\partial B}{\partial S} + B\frac{\partial\theta}{\partial N}\right)\right] = 0, \qquad (2.39)$$

$$\frac{\mathrm{d}A}{\mathrm{d}t} + (A - C)\frac{\partial A}{\partial N} + \frac{1}{\rho}\frac{\partial P}{\partial N} + B\left[\frac{\mathrm{d}\theta}{\mathrm{d}t} + (A - C)\frac{\partial\theta}{\partial N} + \frac{\partial A}{\partial S} + B\frac{\partial\theta}{\partial S}\right] = 0, \qquad (2.40)$$
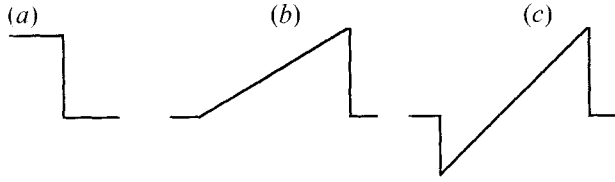
FIGURE 2. Typical shock waveforms (profiles of density or pressure are shown). (a) Step shock, $\partial\mu/\partial N = 0$, (b) Sawtooth, $\partial\mu/\partial N > 0$, (c) N-wave, $\partial\mu/\partial N > 0$.

$$\frac{\mathrm{d}\theta}{\mathrm{d}t} + (A - C)\frac{\partial\theta}{\partial N} - \left(\frac{A - C}{A}\right)\frac{\partial B}{\partial N} - \frac{1}{\rho A}\frac{\partial P}{\partial S} - \frac{1}{A}\left[\frac{\mathrm{d}B}{\mathrm{d}t} + B\frac{\partial B}{\partial S} - AB\frac{\partial\theta}{\partial S}\right] = 0, \quad (2.41)$$

$$\frac{\mathrm{d}P}{\mathrm{d}t} + (A - C)\frac{\partial P}{\partial N} - \frac{\gamma P}{\rho}\left(\frac{\mathrm{d}\rho}{\mathrm{d}t} + (A - C)\frac{\partial\rho}{\partial N}\right) + B\left[\frac{\partial P}{\partial S} - \frac{\gamma P}{\rho}\frac{\partial\rho}{\partial S}\right] = 0. \quad (2.42)$$

On the shock surface Ω the tangential and time derivatives (which are 'interior' derivatives along the shock) and downstream quantities may be expressed using the Rankine–Hugoniot relations (2.26)–(2.29). The normal derivatives, however, are 'exterior' derivatives and can only be found by solving the gasdynamic equations (2.39)–(2.42).

Writing (2.39)–(2.42) ahead of and behind the shock and subtracting, we can eliminate the unknowns $\partial A_b/\partial N$ and $\partial P_b/\partial N$ and derive an equation for the evolution of shock strength, $\mathrm{d}\mu/\mathrm{d}t$. After some manipulation, neglecting terms of $O(\mu^2)$ and normalizing by the length $1/k$ and by the time $1/(a_0 k)$ (where k is a wavenumber characteristic of the flow ahead of the shock, or initial curvature of a shock if the flow is uniform) we find

$$\frac{\mathrm{d}\mu}{\mathrm{d}t} = \frac{1}{2}\left[\frac{\partial\theta}{\partial S} - \frac{(\gamma + 1)}{2}\frac{\partial\mu}{\partial N}\right]\mu - \tilde{B}_a\frac{\partial\mu}{\partial S} - \frac{1}{2}\tilde{e}_{a_{NN}}\mu, \quad (2.43)$$

where $\partial\theta/\partial S$ is the curvature of the shock, and

$$\tilde{e}_{a_{NN}} = n_1^2\tilde{e}_{a_{11}} + 2n_1 n_2\tilde{e}_{a_{12}} + n_2^2\tilde{e}_{a_{22}}, \quad (2.44)$$

$$\tilde{e}_{a_{ij}} = \frac{1}{2}\left(\frac{\partial\tilde{u}_{a_i}}{\partial x_j} + \frac{\partial\tilde{u}_{a_j}}{\partial x_i}\right) \quad (2.45)$$

is the rate of strain in the direction normal to the shock front. The acoustic approximation has only been used to write gradients of pressure ahead of the shock and density in terms of the velocity ahead of the shock and to put $a = a_0$. Note that terms of order M_U^2 would not appear without a factor μ since such terms cancel when the equations (2.39)–(2.42) written ahead of and behind the shock are subtracted.

The first term on the right-hand side of equation (2.43) represents the evolution of shock strength due to the strength and shape of the shock itself. The shock strengthens where it is concave and weakens where it is convex. The term involving $\partial\mu/\partial N$ shows the effect of the flow behind the shock. The shock weakens if $\partial\mu/\partial N > 0$ as in a sawtooth or N-wave (see figure 2). The other terms give the effect of the flow ahead on shock strength.

The presence of $\partial\mu/\partial N$ in (2.43) shows that the first compatibility equation is not closed: we require a second compatibility equation describing the evolution of $\partial\mu/\partial N$.

To derive the second compatibility equation we first take the normal derivative of the conservation equations for mass, momentum and energy. After some manipulation

this produces the following equations:

$$\frac{\mathrm{d}}{\mathrm{d}t}\left(\frac{\partial\rho}{\partial N}\right) + (A-C)\frac{\partial^2 A}{\partial N^2} + \rho\frac{\partial^2 A}{\partial N^2} + \rho\frac{\partial}{\partial S}\left(\frac{\partial B}{\partial N}\right) - \rho A\frac{\partial}{\partial S}\left(\frac{\partial\theta}{\partial N}\right)$$

$$+ \left(2\frac{\partial A}{\partial N} - A\frac{\partial\theta}{\partial S}\right)\frac{\partial\rho}{\partial N} + \left(\frac{\mathrm{d}\theta}{\mathrm{d}t} - C\frac{\partial\theta}{\partial N} + \frac{\partial B}{\partial N}\right)\frac{\partial\rho}{\partial S} + 2\rho\frac{\partial B}{\partial N}\frac{\partial\theta}{\partial N}$$

$$- \rho A\left(\frac{\partial\theta}{\partial N}\right)^2 - \rho A\left(\frac{\partial\theta}{\partial S}\right)^2 - \rho\frac{\partial A}{\partial N}\frac{\partial\theta}{\partial S} + B\left[2\frac{\partial\rho}{\partial N}\frac{\partial\theta}{\partial N} + \rho\frac{\partial^2\theta}{\partial N^2}\right.$$

$$\left. + \frac{\partial}{\partial S}\left(\frac{\partial\rho}{\partial N}\right) + \frac{\partial\theta}{\partial S}\frac{\partial\rho}{\partial S}\right] + \frac{\partial B}{\partial S}\left[\frac{\partial\rho}{\partial N} + \rho\frac{\partial\theta}{\partial S}\right] = 0, \qquad (2.46)$$

$$\frac{\mathrm{d}}{\mathrm{d}t}\left(\frac{\partial A}{\partial N}\right) + (A-C)\frac{\partial^2 A}{\partial N^2} + \frac{1}{\rho}\frac{\partial^2 P}{\partial N^2} + \left(\frac{\mathrm{d}\theta}{\mathrm{d}t} - C\frac{\partial\theta}{\partial N} + \frac{\partial B}{\partial N}\right)\frac{\partial A}{\partial S}$$

$$+ \left(\frac{\partial A}{\partial N}\right)^2 + \frac{\partial B}{\partial N}\left(\frac{\mathrm{d}\theta}{\mathrm{d}t} + (A-C)\frac{\partial\theta}{\partial N}\right)$$

$$+ \frac{1}{\rho}\frac{\partial\rho}{\partial N}\left(\frac{\mathrm{d}A}{\mathrm{d}t} + (A-C)\frac{\partial A}{\partial N}\right) + B\left[\frac{\mathrm{d}}{\mathrm{d}t}\left(\frac{\partial\theta}{\partial N}\right) + \frac{\mathrm{d}\theta}{\mathrm{d}t}\frac{\partial\theta}{\partial S} - C\frac{\partial\theta}{\partial N}\frac{\partial\theta}{\partial S}\right.$$

$$+ 2\frac{\partial A}{\partial N}\frac{\partial\theta}{\partial N} + (A-C)\frac{\partial^2\theta}{\partial N^2} + \frac{\partial}{\partial S}\left(\frac{\partial A}{\partial N}\right) + \frac{\partial\theta}{\partial S}\frac{\partial A}{\partial S}$$

$$\left. + 2\frac{\partial B}{\partial N}\frac{\partial\theta}{\partial S} + B\frac{\partial}{\partial S}\left(\frac{\partial\theta}{\partial N}\right) + B\left(\frac{\partial\theta}{\partial S}\right)^2 + B\left(\frac{\partial\theta}{\partial N}\right)^2\right] = 0, \qquad (2.47)$$

$$\frac{\mathrm{d}}{\mathrm{d}t}\left(\frac{\partial P}{\partial N}\right) - a^2\frac{\mathrm{d}}{\mathrm{d}t}\left(\frac{\partial\rho}{\partial N}\right) + (A-C)\left(\frac{\partial^2 P}{\partial N^2} - a^2\frac{\partial^2\rho}{\partial N^2}\right) + \left(\frac{\mathrm{d}\theta}{\mathrm{d}t} - C\frac{\partial\theta}{\partial N}\right)$$

$$\times\left(\frac{\partial P}{\partial S} - a^2\frac{\partial\rho}{\partial S}\right) + \frac{\partial A}{\partial N}\left(\frac{\partial P}{\partial N} - a^2\frac{\partial\rho}{\partial N}\right) + \frac{\partial B}{\partial N}\left(\frac{\partial P}{\partial S} - a^2\frac{\partial\rho}{\partial S}\right)$$

$$- \gamma\left(\frac{1}{\rho}\frac{\partial P}{\partial N} - \frac{P}{\rho^2}\frac{\partial\rho}{\partial N}\right)\left(\frac{\mathrm{d}\rho}{\mathrm{d}t} + (A-C)\frac{\partial\rho}{\partial N}\right)$$

$$+ B\left[\frac{\partial}{\partial S}\left(\frac{\partial P}{\partial N}\right) - a^2\frac{\partial}{\partial S}\left(\frac{\partial\rho}{\partial N}\right) + \frac{\partial\theta}{\partial S}\left(\frac{\partial P}{\partial S} - a^2\frac{\partial\rho}{\partial S}\right)\right.$$

$$\left. + \frac{\partial\theta}{\partial N}\left(\frac{\partial P}{\partial N} - a^2\frac{\partial\rho}{\partial N}\right) - 2a\frac{\partial a}{\partial N}\frac{\partial\rho}{\partial S}\right] = 0. \qquad (2.48)$$

A fourth equation corresponding to (2.41) is required only to evaluate the third compatibility equation. In order to close the first compatibility equation we require an $O(1)$ equation for $\mathrm{d}\mu/\mathrm{d}N$. The zeroth-order equation for $\mathrm{d}\mu/\mathrm{d}N$ can be obtained from (2.46)–(2.48) by subtracting the these equations written ahead of and behind the shock and then eliminating $\partial^2 A_b/\partial N^2$ and $\partial^2 P_b/\partial N^2$ while retaining only terms of $O(1)$.

The resulting second compatibility equation is

$$\frac{\mathrm{d}}{\mathrm{d}t}\left(\frac{\partial\mu}{\partial N}\right) = \frac{1}{2}\left[\frac{\partial\theta}{\partial S} - (\gamma+1)\frac{\partial\mu}{\partial N}\right]\frac{\partial\mu}{\partial N} - \tfrac{3}{2}\tilde{e}_{a_{NN}}\frac{\partial\mu}{\partial N}. \qquad (2.49)$$

One notices immediately that equation (2.49) does not contain any terms involving

$\partial^2\mu/\partial N^2$ and thus the system of compatibility equations for weak shocks is closed at the second compatibility equation. This level of approximation is equivalent to a description of the flow behind the shock in terms of a first-order Taylor expansion around the instantaneous shock position. Note that the derivation is only valid if $\partial\mu/\partial N$ and higher-order derivatives are $O(1)$ and that $\partial\mu/\partial S = O(\mu)$; however Ravindran, Sunder & Prasad (1994) have shown that if $\partial\mu/\partial N > 0$ the first-order approximation will always give accurate results.

The two compatibility equations (2.43) and (2.49) together with the SME (e.g. (2.13)) form a closed set of equations governing the propagation of a weak shock into a flow in subsonic, non-uniform motion. The domain of validity of the theory is that given by (2.8). In general the theory will also be limited in time because remote disturbances may catch up with the shock from behind and the effect of these disturbances cannot be included in the truncated Taylor expansion used to describe the flow behind the shock. The comparison with DNS in the following section shows that, the time limitation is not significant for the time scales considered in this paper.

The present solution of the shock propagation problem is limited to two-dimensional motion, but this approach can in principle be extended to three dimensions. Only one shock front can be resolved, or equivalently, the shock front must remain smooth. Any additional shock fronts (such as the Mach stems that develop at a shock-shock after focusing) are not included in this theory, but their effects may be found using additional methods (see §4). These first-order equations will be the ones used for computing shock propagation in non-uniform flows. Note that although we retain only first-order terms in μ, the factor $(\gamma + 1)/4$ multiplying μ in the SME and first compatibility equation is less than 1 (e.g. $(\gamma + 1)/4 = 0.6$ if $\gamma = 1.4$) and so the approximation may be sufficient for μ quite close to 1 in practice. If the magnitude of the terms ahead of the shock is less than μ, then the terms ahead of the shock in the first and second compatibility conditions may be neglected.

2.3. *The second-order approximation*

In order to check whether qualitatively new effects result from retaining higher-order terms we have derived the second-order shock propagation equations, retaining terms up to $O(\mu^2)$. Following the method described in §2.2 we have derived the second-order SME and compatibility equations. Since the second-order approximation will only be used to check the first-order approximation, we assume for simplicity that gradients of quantities ahead of the shock are $O(\mu)$ and choose the test field appropriately. The resulting shock equations are

$$\frac{\partial g}{\partial t} = \tilde{u}_a - \tilde{v}_a\frac{\partial g}{\partial y} + \left(1 + \frac{(\gamma + 1)}{4}\mu - \frac{(\gamma + 1)(5 - 3\gamma)}{32}\mu^2\right)\left(1 + \left(\frac{\partial g}{\partial y}\right)^2\right)^{1/2}, \quad (2.50)$$

$$\frac{d\mu}{dt} = \frac{1}{2}\left[\left(\frac{\partial\theta}{\partial S} - \frac{(\gamma + 1)}{2}\frac{\partial\mu}{\partial N}\right) + \frac{(\gamma + 1)}{8}\left(\frac{\partial\theta}{\partial S} + \frac{(7 - \gamma)}{2}\frac{\partial\mu}{\partial N}\right)\mu\right]\mu - \tilde{B}_a\frac{\partial\mu}{\partial S} - \tfrac{1}{2}\tilde{e}_{a_{NN}}\mu,$$

$$(2.51)$$

$$\frac{\mathrm{d}}{\mathrm{d}t}\left(\frac{\partial\mu}{\partial N}\right) = \frac{1}{2}\left[\left(\frac{\partial\theta}{\partial S} - (\gamma+1)\frac{\partial\mu}{\partial N}\right)\frac{\partial\mu}{\partial N} + \frac{(\gamma+1)(3-\gamma)}{2}\left(\frac{\partial\mu}{\partial N}\right)^2\mu\right.$$

$$\left. - \frac{(3-\gamma)}{4}\frac{\partial\theta}{\partial S}\frac{\partial\mu}{\partial N}\mu + \frac{3}{4}\left(\frac{\partial\theta}{\partial S}\right)^2 - \frac{\partial^2\mu}{\partial S^2} - \frac{(\gamma+1)}{2}\frac{\partial^2\mu}{\partial N^2}\mu\right] - \frac{3}{2}\tilde{e}_{a_{NN}}\frac{\partial\mu}{\partial N},$$

$$(2.52)$$

$$\frac{\mathrm{d}}{\mathrm{d}t}\left(\frac{\partial^2\mu}{\partial N^2}\right) = \frac{1}{2}\left[\frac{(5+2\gamma-\gamma^2)}{2}\left(\frac{\partial\mu}{\partial N}\right)^3 + \left(\frac{\partial\theta}{\partial S} - 3(\gamma+1)\frac{\partial\mu}{\partial N}\right)\frac{\partial^2\mu}{\partial N^2}\right.$$

$$\left. + \frac{7}{4}\left(\frac{\partial\theta}{\partial S} - \frac{(3-\gamma)}{7}\frac{\partial\mu}{\partial N}\right)\frac{\partial\theta}{\partial S}\frac{\partial\mu}{\partial N}\right].$$

$$(2.53)$$

Note that the second-order equations involve *three* compatibility conditions. It is tempting to suppose that an Nth-order weak shock approximation will require $N+1$ compatibility equations. The terms ahead of the shock have exact μ or $\partial\mu/\partial N$ factors, hence no new upstream terms appear in the SME or first and second compatibility equations. The factor multiplying μ^2 in the SME is only 0.06 (for $\gamma = 1.4$) which suggests that this approximation should be sufficient even for μ close to 1.

The second-order equations governing the motion of points on the shock surface are

$$\frac{\mathrm{d}X}{\mathrm{d}t} = N_1\left(1 + \frac{(\gamma+1)}{4}\mu - \frac{(\gamma+1)(5-3\gamma)}{32}\mu^2\right) + \tilde{u}_a, \qquad (2.54)$$

$$\frac{\mathrm{d}Y}{\mathrm{d}t} = N_2\left(1 + \frac{(\gamma+1)}{4}\mu - \frac{(\gamma+1)(5-3\gamma)}{32}\mu^2\right) + \tilde{v}_a, \qquad (2.55)$$

$$\frac{\mathrm{d}\theta}{\mathrm{d}t} = \frac{(\gamma+1)}{4}\left(1 - \frac{(5-3\gamma)}{4}\mu\right)\frac{\partial\mu}{\partial S} + N_1\frac{\partial\tilde{u}_a}{\partial S} + N_2\frac{\partial\tilde{v}_a}{\partial S}. \qquad (2.56)$$

3. Numerical method

The system of nonlinear equations (2.13), (2.43) and (2.49) governing the propagation of a weak shock in a non-uniform flow cannot be solved analytically except in special cases. In general, we require a numerical method to calculate the evolution of the shock.

The simplest way of calculating the spatial derivatives for periodic boundary conditions is to discretize uniformly $g(y,t)$ in y and use a fast Fourier transform (FFT) method to calculate the spatial derivatives. However, one of the problems we wish to consider is the focusing of weak shocks. In order to answer questions such as whether one or two shock-shocks form at the focus we need to resolve regions of high shock strength extremely finely. This requirement suggests that an adaptive, non-uniform discretization of the shock is needed. FFT methods are incapable of dealing with non-uniform grids and hence to investigate shock focusing we require a different method of calculating spatial derivatives.

A natural way to resolve the shock is to discretize its arclength and then follow the motion of points on the shock surface. As the shock evolves these points move towards regions of high strength, thus resolving more finely regions near a focus and regions where (concave) curvature is high. Using this method the shock is 're-gridded' automatically at each time step by the dynamical equations of the shock itself at no

extra computational cost. A further advantage of this description is that it allows for the possibility of the shock overturning (i.e. the equation of the shock is then given by $x = g(x, y, t)$). Although it is unlikely that a shock will actually overturn even in a two-dimensional velocity field, flame fronts do often overturn (because of their slower propagation speed). Because the propagation of shocks and flame fronts is very similar, allowing for overturning of the front means that this method can be carried over with only minor modifications to the case of flamelets. Note that the use of compatibility conditions with the 'field equation' avoids the problem of loops forming in the front encountered by Vassilicos & Hunt (1992).

Instead of the SME (2.13) we follow the shock using the 'shock ray' equations (2.30) where the unit normal is

$$(N_1, N_2) = \frac{(Y_S, -X_S)}{(X_S^2 + Y_S^2)^{1/2}},$$ (3.1)

and the curvature is

$$\frac{\partial \theta}{\partial S} = \frac{X_{SS} Y_S - X_S Y_{SS}}{(X_S^2 + Y_S^2)^{3/2}}.$$ (3.2)

Note that if the gradients ahead of the shock are very weak the terms in the second and third compatibility equations depending on gradients of quantities ahead of the shock may be neglected. The spatial derivatives X_S, X_{SS} etc. are calculated using second-order central finite differences on a non-uniform grid:

$$X_S = \frac{-b^2 X_{i-1} - (a^2 - b^2) X_i + a^2 X_{i+1}}{(a^2 b + ab^2)},$$ (3.3)

$$X_{SS} = \frac{b X_{i-1} - (a + b) X_i + a X_{i+1}}{\frac{1}{2}(a^2 b + ab^2)}$$ (3.4)

where

$$a = \Delta S_{i-1} = S_i - S_{i-1},$$
$$b = \Delta S_i = S_{i+1} - S_i,$$
$$c = \Delta S_{i-2} + \Delta S_{i-1} = S_i - S_{i-1},$$
$$d = \Delta S_i + \Delta S_{i+1} = S_{i+2} - S_i.$$

If the flow or initial conditions are non-periodic (as in the case of an initially parabolic shock) the spatial derivatives at the end points of the shock are calculated using backwards or forwards differences.

The arclength increments are calculated by assuming that adjacent points are joined by straight lines, i.e.

$$\Delta S_i = \left[(X_i - X_{i-1})^2 + (Y_i - Y_{i-1})^2 \right]^{1/2}.$$ (3.5)

No significant improvement was found if more sophisticated methods were used to calculate arclength increments (e.g. polynomial interpolation).

The shock equations were stepped forward in time using a variable-step-size Adams method (NAG subroutine d02cbf). This routine allows the simultaneous solution of a system of equations (one for each grid point for each of the shock equations). The routine automatically adjusts the step size during the integration to attain the specified accuracy.

The shock was discretized using 256 points and it was checked that doubling the number of points did not change the result significantly. The non-uniform grid
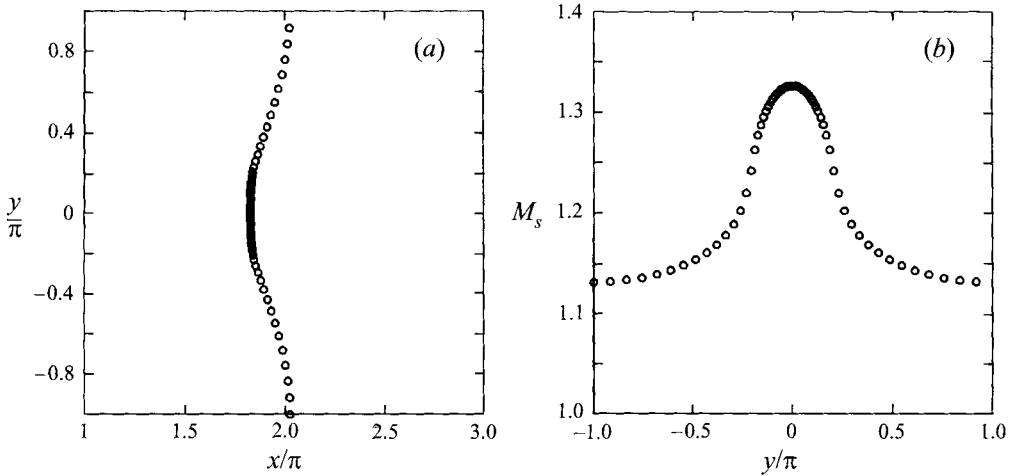
FIGURE 3. An illustration of the way the non-uniform grid points concentrate in regions of high shock strength (every fourth point is plotted). The flow ahead of the shock is sinusoidal, $u(x, y) = -0.1 \cos y$, $v(x, y) = 0$, the initial shock strength $M_{S0} = 1.2$ and $t = 5.0$ (normalized by $1/(a_0 k)$). (a) Shock front. (b) Shock strength $M_S = 1 + (\gamma + 1)/4\mu$.

method was checked against the FFT method for a sinusoidal velocity field ahead of the shock. For relatively short times (before large differences in strength develop) there was no significant difference between solutions obtained using the two methods. The FFT method had problems resolving the shape of the shock near the focus due to Gibbs oscillations. Figure 3 shows how the grid points concentrate in areas of high shock strength/curvature.

Running on a SUN sparcstation, the shock program takes only a few minutes to evolve the shock until focus (e.g. using an initially parabolic shock, or sinusoidal shear flow). This method's low computational cost makes it a good candidate for significantly reducing the running times in a DNS of the shock–turbulence interaction by eliminating the need to resolve the internal structure of the shock.

4. Verification of the theory

In this section we verify the first-order shock equations against established asymptotic weak shock results for decaying N-waves and expanding cylindrical shock waves. The equations we obtain are original.

The first- and second-order numerical solutions for an initially plane shock wave in a sinusoidal shear flow are compared to a DNS of the same flow. The solutions are compared after focusing – an extreme test since the approximations used in deriving the shock propagation equations are not strictly satisfied after shock-shocks develop. This test also checks the validity of treating the shock as a discontinuity since the DNS actually resolves the internal structure of the shock. A method for extending the solution past the time shock-shocks form is also tested.

Finally, we attempt to derive the Guderley self-similarity solution for an expanding strong shock as a strong shock limit of our second-order solution for moderately weak shocks.

4.1. *N-wave*

Consider a plane shock with an N-wave profile (see figure 2) propagating into a fluid at rest. In this case the first-order approximations to the compatibility equations (2.43) and (2.49) become

$$\frac{d\mu}{dt} = -\tfrac{1}{4}(\gamma + 1)\mu_1(t)\mu(t),$$ (4.1)

$$\frac{d\mu_1}{dt} = -\tfrac{1}{2}(\gamma + 1)\mu_1(t)^2,$$ (4.2)

where $\mu_1 = \partial\mu/\partial N$, and $X(t)$ is the position of the shock. The initial conditions corresponding to an N-wave (or sawtooth wave) are

$$\mu(0) = \mu_0,$$ (4.3)

$$\mu_1(0) = \mu_{10} > 0.$$ (4.4)

The second compatibility equation (4.2) can be integrated at once giving

$$\mu_1(t) = \mu_{10}\left(1 + \tfrac{1}{2}(\gamma + 1)\mu_{10}t\right)^{-1}.$$ (4.5)

Thus, the slope of the N-wave decreases like t^{-1} for large times. The shock strength can now be found by substituting the solution (4.5) into the first compatibility equation (4.1) and integrating:

$$\mu(t) = \mu_0\left(1 + \tfrac{1}{2}(\gamma + 1)\mu_{10}t\right)^{-1/2},$$ (4.6)

and we see that shock strength decreases like $t^{-1/2}$ for large times. Since $\mu \propto t^{-1/2}$ and $\mu_1 \propto t^{-1}$, the width of the N-wave must increase like $t^{1/2}$. These results agree with those obtained by Courant & Friedrichs (1948, pp. 164–168) and by Whitham (1974, pp. 312–322) using his weak shock theory for the decay of a two-dimensional N-wave. Note that if $\mu_{10} = 0$ the plane shock does not decay.

4.2. *Expanding cylindrical shock*

Now consider a cylindrical shock expanding into a fluid at rest. The shock equations become

$$\frac{dR}{dt} = 1 + \tfrac{1}{4}(\gamma + 1)\mu(t),$$ (4.7)

$$\frac{d\mu}{dt} = \frac{1}{2}\left(-\frac{1}{R(t)} - \tfrac{1}{2}(\gamma + 1)\mu_1(t)\right)\mu(t),$$ (4.8)

$$\frac{d\mu_1}{dt} = \frac{1}{2}\left(-\frac{1}{R(t)} - (\gamma + 1)\mu_1(t)\right)\mu_1(t),$$ (4.9)

where $R(t)$ is the radius of the shock and we have used the fact that the curvature is $1/R(t)$ by symmetry. The initial conditions are the same as for the N-wave (4.3) and (4.4).

From equation (4.7) $R(t) = t + O(\mu)$. Using the weak shock approximation we need only take the $O(1)$ solution for the shock radius in equations (4.8) and (4.9), i.e. we take $R(t) = t$. Then by inspection the second compatibility equation (4.9) has the solution

$$\mu_1(t) \propto \frac{1}{(\gamma + 1)}t^{-1},$$ (4.10)

which is the same as for the plane N-wave. If $R(t) = t$ and the solution (4.10) are
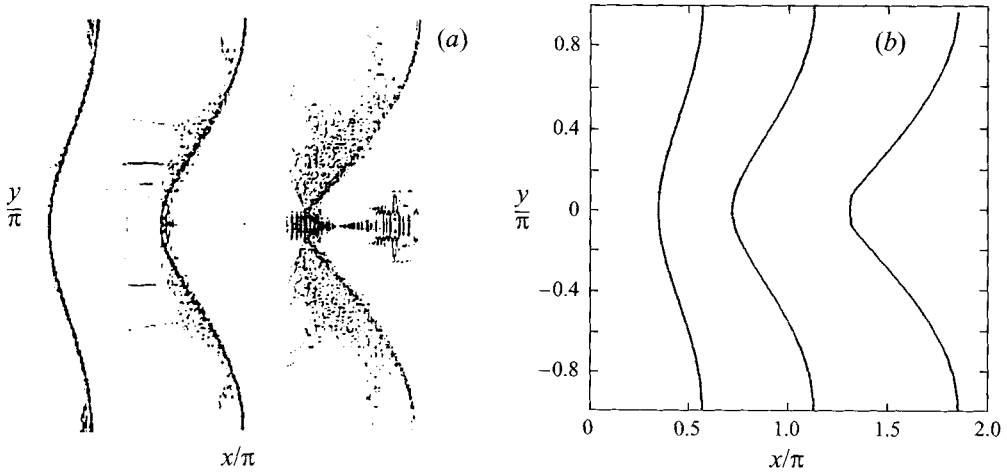
FIGURE 4. The evolution of an initially straight shock $M_{S0} = 1.2$ in a sinusoidal shear flow $\tilde{u}_a(x, y, t) = -0.3 \cos y, \tilde{v}_a(x, y, t) = 0$ at times $t = 0$, 1.2, 2.4, 4.0. (a) Calculated using DNS (the lines are contours of dilatation). (b) Calculated by solving numerically the second-order shock equations.

substituted into the first compatibility equation (4.8) one obtains the equation

$$\frac{d\mu}{dt} = -\frac{3}{4}\frac{\mu}{t}, \tag{4.11}$$

which can then be integrated giving

$$\mu(t) \propto t^{-3/4}, \tag{4.12}$$

and we see that the strength of an expanding cylindrical shock decays like $t^{-3/4}$. This result agrees with that obtained by Landau (1945) for expanding cylindrical weak shocks.

Since $\mu \propto t^{-3/4}$ and $\mu_1 \propto t^{-1}$, the width of the N-wave behind the cylindrical shock must increase like $t^{1/4}$.

Note that for both cylindrical shocks and plane N-waves the 'shock rays' remain straight lines because of symmetry, and hence the weak shock theory assumption that shock geometry is given by geometrical acoustics is satisfied exactly. In the following section we check the shock equations in the case of shock focusing in a sinusoidal field: a case where weak shock theory fails.

4.3. *Sinusoidal shear flow, comparison with DNS*

The previous two examples involved shocks propagating into a uniform flow and the symmetry of the problems ensured that the 'shock rays' remained straight lines. We now consider the case of an initially straight shock propagating into a steady sinusoidal velocity field specified by

$$\tilde{u}_a(x, y) = -0.3 \cos y, \tag{4.13}$$

$$\tilde{v}_a(x, y) = 0. \tag{4.14}$$

The initial shock strength $M_{S0} = 1.2$ and the shock wave has a step profile. This situation is examined in more detail in §5.2. The non-uniformity of the flow ahead of the shock eventually causes the shock to *focus* around $y = 0$ at $t = T_C$ and form two shock-shocks (discontinuities in shock strength) separated by a flat shock disk. Associated with the shock-shocks are Mach stems (secondary shocks) and vortex
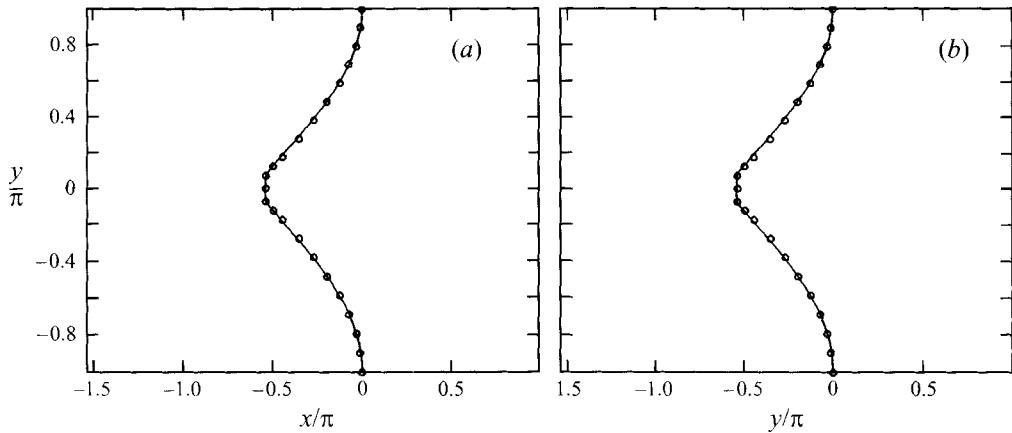
FIGURE 5. Comparison of shock shape in a sinusoidal shear flow $\tilde{u}_a(x, y, t) = -0.3 \cos y$, $\tilde{v}_a(x, y, t) = 0$ at $t = 4.0$ (after focus) predicted by the shock equations (solid line) and calculated from DNS (circles) ($M_{S0} = 1.2$). The diameter of the circles is roughly the width of the DNS shock. (*a*) Second order. (*b*) First order, obtained by extending 'wings' and shock disk separately from $T = 3.7$.

sheets in the flow behind the shock. The 'shock rays' are curved in this case and weak shock theory fails, predicting infinite shock strength at the focus.

The evolution of the shock front calculated using DNS (a program written by S. Lee at CTR, Stanford University) and by solving numerically the second-order shock equations are shown in figures 4(*a*) and 4(*b*) respectively. A comparison of the shock shape predicted by the shock equations and by DNS after shock-shocks form is a severe test because in deriving the shock equations we assumed that $\partial \mu / \partial S$ remains $O(\mu)$. Figure 5(*a*) shows a comparison of shock position after focus from the DNS and the shock equations. The agreement is remarkably good: the error is certainly less than the thickness of the shock front.

Note that the approximation $\partial \mu / \partial S = O(\mu)$ used in deriving the shock equations becomes invalid slightly before T_C (when the more fundamental assumptions that only a single shock exists in the flow and that the shock surface is smooth become invalid). However, the comparison with DNS has shown that the first-order equations give the correct shock shape even at $t = T_C$. This somewhat surprising result may be explained by the fact that the curvature increases at the same rate as $\partial \mu / \partial S$ once the curvature becomes large. Thus the curvature always remains the dominant term in the compatibility equations (2.43) and (2.49).

The first-order solution breaks down when the shock focuses and discontinuities in shock strength ('shock-shocks') form at $T_C = 3.3$, before the time of the DNS data at $t = 4.0$. The discontinuous jump in M_S means that the shock surface has an associated corner or 'kink'. The jump in shock strength behaves like a normal shock and propagates along the shock at a speed that depends on the size of the jump and the angle between the shock disk and the outer shock 'wing'. The shock system at a focus is essentially the same as that of a Mach reflection (e.g. supersonic flow in a nozzle, see Courant & Friedrichs 1948, p. 387). In both cases a shock-shock forms and the 'shock-disk' and the 'wing shock' coalesce to form a single stronger shock (reflected wave) behind. A vortex sheet also forms behind the shock (see Kevlahan 1996 for a discussion of the vorticity jump across a shock). The shock system at a Mach reflection is shown in figure 6(*a*).

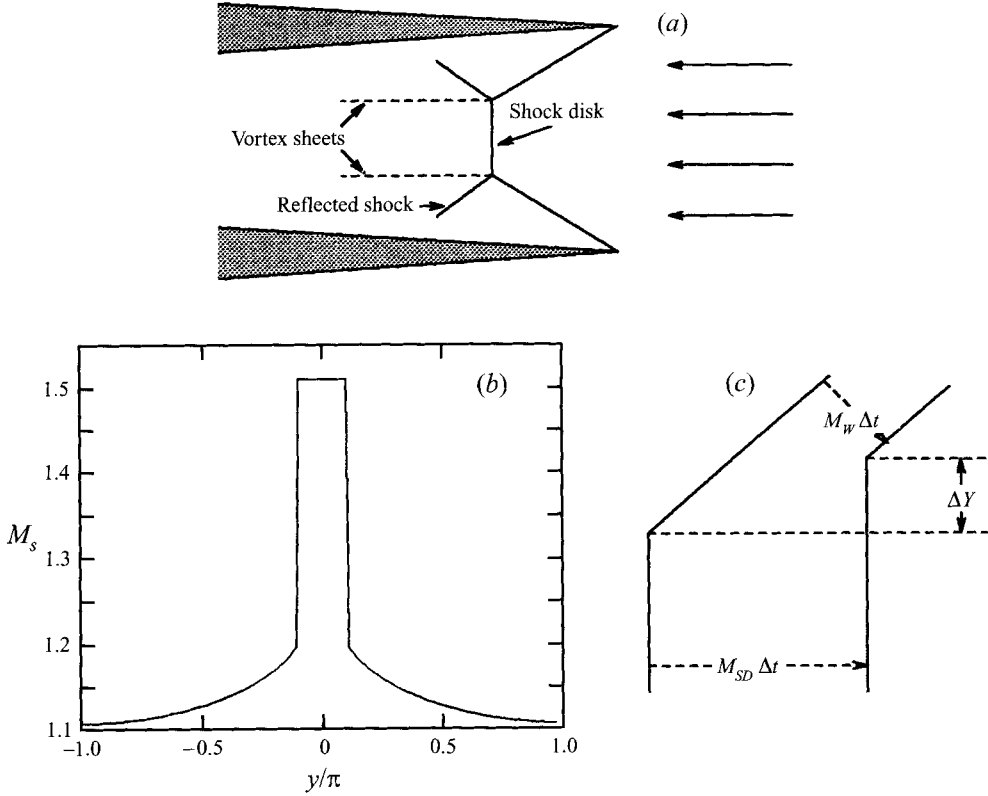The solution actually only breaks down at the two shock-shock points; at all other

FIGURE 6. (a) The shock system at a Mach reflection in stationary flow between parallel wedges (after Courant & Friedrichs 1948, p. 337). (b) Mach number M_S of a shock in sinusoidal shear flow at $t = 3.7$ showing shock-shocks (M_S in the shock disk has been replaced by its value at $y = 0$). (c) Construction used to propagate a shock after the focus when shock-shocks form.

places the shock remains smooth and the curvature, $\partial\mu/\partial S$ and $\partial\mu/\partial N$ is small. This means that $d\mu/dt$ is small and suggests that the shape and strength of the shock disk and wings may have reached an approximately stationary state. Subsequent changes in the shock system reduce to an increase or decrease in size of the shock disk determined by the strength of the shock-shock and by the angle between the shock disk and the wings (see the experimental photos of the focusing of weak shocks in Sturtevant & Kulkarny 1976). At least for short times the angle between the shock disk and wing does not change significantly. Therefore, the solution may be extended for short times past the time kinks form by propagating the shock disk and wing as separate shocks. The position of the kink is then given by the intersection of the two shocks. This method was used by Whitham (1974, p. 289) to treat shock-shocks in his theory of shock dynamics.

For small times the shock can be propagated in two parts using the following approximate solutions to the SME:

$$g_{SD}(t) = M_{SD}t + \tilde{u}_a + g_{SD}(0), \tag{4.15}$$

$$g_W(y,t) = \frac{M_W(y)}{N_1(y)}t + \tilde{u}_a + g_W(y,0), \tag{4.16}$$

where $x = g(y,t)$ gives the position of the shock, M_{SD} is the (uniform) Mach number

of the shock disk at T_C, and $M_W(y)$ is the shock strength of the wings at T_C. The position of the physical shock is then given by $g(y,t) = \max(g_{SD}, g_W)$ (the physical shock is the portion ahead of the intersection). This shock construction is shown schematically in figure 6(c). A comparison of the first-order solution extended from $t = 3.7$ to $t = 4.0$ with the DNS solution at $t = 4.0$ is shown in figure 5(b). The agreement is remarkably good.

The above 'intersection' method could be used for arbitrary times by solving numerically the shock equations for the shock disk and wings separately. This method allows for the possibility that the shape and strength of the shocks could change over time.

The intersection method can also give a rough estimate of whether the two shock-shocks will move apart or together. Figure 6(c) shows that for short times in uniform flow the speed of the shock-shock in the y-direction is

$$C_{SS} \cdot Y = \frac{\Delta Y}{\Delta t} = \frac{N_1}{N_2}\left(M_{SD} + \frac{\Delta M - M_{SD}}{N_1}\right), \tag{4.17}$$

Thus the shock-shocks will move apart if

$$1 - \frac{\Delta M}{M_{SD}} < N_1, \tag{4.18}$$

where ΔM is the jump associated with the shock-shock and N_1 is the x-component of the unit normal to the shock on the wing side of the shock-shock (see figure 6). If the inequality (4.18) is not satisfied the shock-shocks will move together and may eventually close up, leading to the focusing behaviour observed by Sturtevant & Kulkarny (1976) for moderately weak shocks (see their figures 6b and 6c), otherwise the shock-shocks will move apart and 'strong' shock ($M_S = 1.1$–1.3) focusing occurs (Sturtevant & Kulkarny, figure 6d). This criterion will be used in §5.1 which considers the focusing of an initially parabolic shock.

Germain & Guiraud (1966) claimed that the presence of viscosity is a singular perturbation to the Euler equations and must *always* be included in the description of curved shocks. This is equivalent to saying that one may never neglect the thickness of a curved shock when deriving equations governing its propagation. We have shown here that the focusing of a shock in a non-uniform velocity field is described extremely accurately by a theory which assumes that shock thickness is negligible. The shock is extremely curved at the focus (the curvature is infinite at the shock-shocks) and yet the discontinuous shock remains at the centre of the finite-thickness shock calculated using DNS. These results suggest that for practical purposes it is sufficient to consider an unsteady shock to be discontinuous, even if the shock has significant curvature.

In this section we have verified the first-order shock equations against a full DNS that resolves the internal structure of the shock, and have also checked a method for extending the solution past the time of focus. This is an extreme test of the theory and numerical method since the shock strength actually becomes discontinuous at the focus. The shock shape at the focus $t = T_C$ calculated by the first-order equations agrees remarkably well with the shock shape calculated using DNS. The second-order solution shows no qualitative differences from the first-order solution, although discontinuities in μ occur slightly later. Thus the first-order equations may be used right up until the focus, $t = T_C$. After the focus the solution may be extended using the intersection method described in this section.

4.4. *Converging strong shock*

Guderley (1942) found a self-similarity solution for converging cylindrical and spherical strong shocks which has since been confirmed by Van Dyke & Guttmann (1982). The strength of a converging cylindrical strong shock in a uniform flow with $\gamma = 1.4$ varies with radius according to

$$M(r) \propto r^{-n}, \quad n = 0.197294. \tag{4.19}$$

In comparison, $n = 0$ for an acoustic wave.

As another rather extreme test of the shock equations we shall attempt to deduce the value of n from the change in n as the initial shock strength M_{S0} varies between 1 and 1.5. The method is as follows: first, the second-order shock equations are solved numerically for a cylindrical strong shock and $n(M_{S0})$ is determined for a range of shock strengths $1 \leqslant M_{S0} \leqslant 1.5$. Second, it is assumed that $n(M_{S0})$ has the following form:

$$1 - \frac{n(M_{S0})}{n_\infty} \propto M_{S0}^{-b}, \tag{4.20}$$

and n_∞ is altered until the data form the straightest line on a plot of $\log(1-n(M_{S0})/n_\infty)$ versus $\log(M_{S0})$. The value of n_∞ which gives the best fit is the estimate for the Guderley strong shock exponent n.

Using the above procedure n was estimated to be 0.171, within 13.5% of the exact value for the limit of infinite shock strength. The exponent $b = 4.75$. A 13.5% error is actually quite good considering a weak shock theory was used to estimate a result for asymptotically strong shocks! This result indicates that the second-order shock equations contain a significant amount of strong shock physics.

It is also interesting to note that for a shock of only $M_{S0} = 1.5$ n is within about 10% of its value in the limit of infinite shock strength.

5. Applications

In this section the first-order shock equations that were derived and verified in the previous three sections are applied to a variety of shock propagation problems. The focusing of an initially parabolic shock in a uniform flow is considered in §5.1, then an initially straight shock propagating into various non-uniform flows exhibiting some fundamental properties of turbulence are considered. The flows ahead of the shock considered are: a sinusoidal shear flow (§5.2), a vortex array (§5.3), and an array of point vortices (§5.4). Two-scale versions of the sinusoidal and vortex array flows are also examined to determine whether the shock deforms on the energetic scale or the vortical scale of the flow.

5.1. *The focusing of an initially parabolic shock*

An acoustic discontinuity ($M_S = 1$) with an initially parabolic profile will eventually come to a perfect focus at a distance equal to the radius of curvature on its axis. Weak shock theory assumes that a weak shock focuses in the same way as an acoustic discontinuity and hence predicts infinite strength at the focus (where ray tube area vanishes).

Sturtevant & Kulkarny (1976) examined experimentally the focusing of weak shock waves. They found that the geometry of the shocks at the focus is different from that predicted by weak shock theory, and that (as might be expected) the shock strength

remains finite. At the focus relatively strong ($M_S \approx 1.2$) shocks show a flat shock disk bounded by shock-shocks which gradually move apart. If the shock is slightly weaker the shock-shocks move together and eventually meet, producing the crossed shocks predicted by geometrical acoustics theory. They emphasize that in both cases the behaviour at the focus is nonlinear.

In this section we examine the problem of the focusing of an initially parabolic shock in detail. The parabolic shock is propagated until the time of focus by numerically solving the first-order shock equations. Some of the questions we address are: How does the separation of shock-shocks depend on initial shock strength? How does the maximum shock strength depend on the initial shock strength? What is the critical Mach number defining the transition between crossed and uncrossed shocks? How does the time at which shock-shocks form (the time of focus, T_C) depend on the initial shock strength?

Initially the shock is parabolic in shape, i.e.

$$X_0 = \tfrac{1}{2} Y_0^2, \quad -1.68 \leqslant Y_0 \leqslant 1.68 \tag{5.1}$$

with constant strength M_{S0}, and a step condition behind the shock $\partial \mu / \partial N = 0$. This initial condition is chosen to reproduce the conditions of experiment number one of Sturtevant & Kulkarny (1976) (a plane shock is reflected off a parabolic cylinder reflector with an angle of convergence of 160°). These initial conditions produce a perfect line focus in the case of acoustic discontinuities. The initial Mach number of the shock M_{S0} is varied between 1 and 1.3.

Figure 7(*a*) shows an acoustic discontinuity ($M_{S0} = 1$) at various times up to focus, while figure 7(*b*) shows a weak shock ($M_{S0} = 1.3$) at equivalent times. The acoustic discontinuity exhibits the type of focusing typical of geometric acoustics, i.e. a single kink appears at $T_C = 1$ at the axis of the initial parabola. The weak shock, on the other hand, focuses at a later time $T_C M_{S0} = 1.17$ and the shape of the shock is very different from the acoustic discontinuity: a straight central section bounded by two kinks. The shape determined here is very similar to that observed experimentally by Sturtevant & Kulkarny (see figure 7*c* which has been reproduced from Sturtevant & Kulkarny).

The origin of the double kinks is made clear by examining the evolution of shock strength which is shown in figure 7(*d*). The shock strength increases steadily at the centre of the shock (where the curvature is greatest) until the the shock strength eventually develops a pair of discontinuities. These discontinuities in shock strength are associated with discontinuities in propagation speed via equation (2.30) and hence with kinks in the shock surface itself. Once the discontinuities form the shock strength no longer increases and this determines the maximum shock strength at the focus, M_{max}.

The discontinuities in shock strength may be thought of as 'shock-shocks', i.e. a shock wave on the shock front, which form when waves carrying shock strength along the shock surface break, just as an acoustic pulse can overturn to form a normal shock. Whitham (1974, pp. 284–291) discussed the formation of shock-shock in the context of his theory of shock dynamics for *strong* shocks, but does not consider the possibility of shock-shocks forming on weak shocks (his weak shock theory does not allow for this). Here we see that the nonlinear phenomenon of shock-shocks is also the basic focusing mechanism in weak shocks.

The separation of the shock-shocks at the focus (when the shock-shocks first form) is an increasing function of initial shock strength. The power-law dependence of
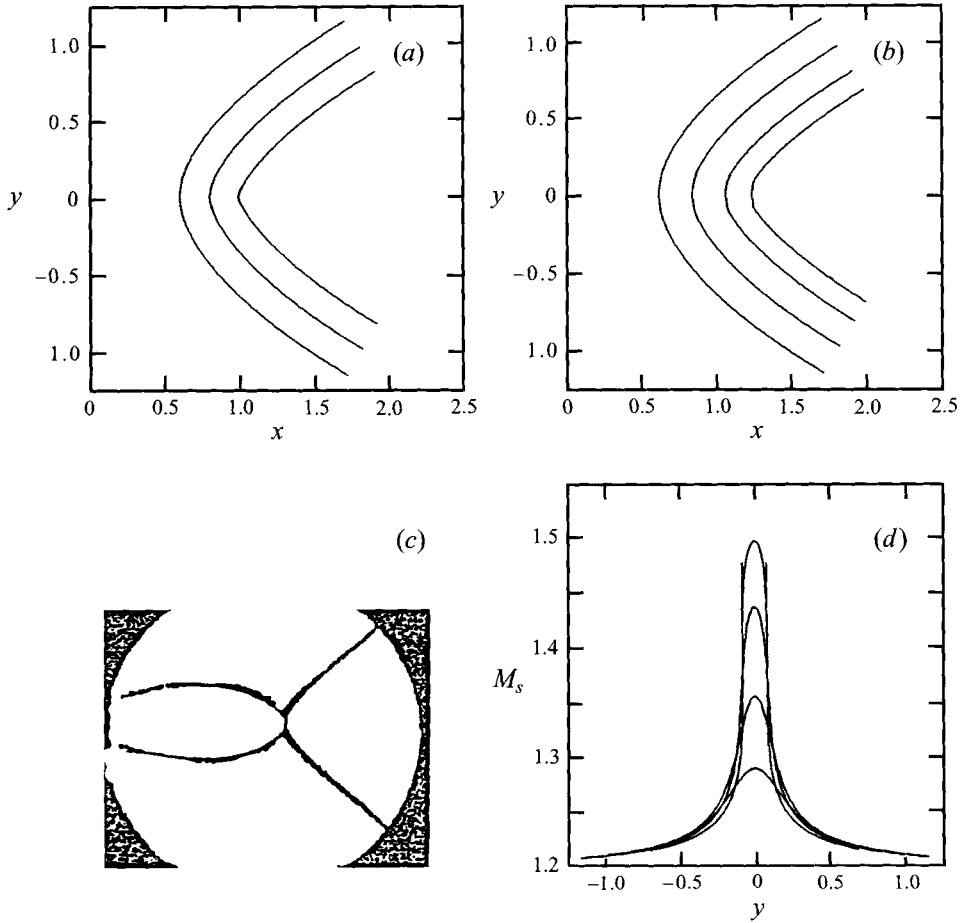
FIGURE 7. Shock focusing (times normalized by multiplying by M_{S0} for comparison purposes). (a) $M_{S0} = 1$ shock (acoustic discontinuity) at times $t = 0.60, 0.80, 1.0$ (focus). (b) $M_{S0} = 1.2$ shock at times $t = 0.60, 0.80, 1.0, 1.14$ (focus). Note the double kinks bounding a flat shock disk. (c) Experimental shock $M_{S0} = 1.2$ at focus (from Sturtevant & Kulkarny 1976, figure 5). (d) Evolution of shock strength for $M_{S0} = 1.2$ shock at times $t = 0.60, 0.80, 1.0, 1.14$. Note the spikes (where the numerical method begins to break down) which indicate the appearance of shock-shocks.

shock-shock separation (ΔY_C) on initial shock strength ($M_{S0} - 1$) is roughly

$$\Delta Y_C \propto (M_{S0} - 1)^{0.8}, \tag{5.2}$$

for $M_{S0} < 1.1$. For $M_{S0} > 1.1$ the ΔY_C increases more slowly. Note that the shock-shock separation is non-zero for all initial strengths $M_{S0} > 1$.

The power-law dependence of shock strength at the focus $(M_{max} - 1)/(M_{S0} - 1)$ on initial shock strength $M_{S0} - 1$ is very close to $-\frac{1}{3}$, i.e.

$$\frac{M_{max} - 1}{M_{S0} - 1} \propto (M_{S0} - 1)^{-1/3}. \tag{5.3}$$

The dependency of the normalized time to focus minus 1 (where an acoustic discontinuity $M_{S0} = 1$ focuses at time 1) on initial shock strength is approximately

$$T_C M_{S0} - 1 \propto (M_{S0} - 1)^{1/2}, \tag{5.4}$$

for $M_{S0} - 1 \leqslant 1.1$. Thus all weak shocks take longer to focus than an acoustic discontinuity.

An indication of whether the shock-shocks will move together and eventually meet, forming a crossed shock front, can be found using the criterion given in equation (4.18). The smallest Mach number for which the criterion is satisfied is $M_C \approx 1.27$, thus one might expect crossed shocks for $M_{S0} < 1.27$ and uncrossed shocks for $M_{S0} \geqslant 1.27$. Sturtevant & Kulkarny find experimentally that $M_C \approx 1.2$. Note that M_C is a fairly rough indication of the type of focusing owing to the difficulty of determining accurately the shock-shock jump, and because it assumes that the strengths of the shock disks and wings do not evolve significantly after focus.

5.2. *Sinusoidal shear flow*

Now we examine a problem complementary to that considered in §5.1: the propagation of an initially plane shock in a non-uniform velocity field. The velocity field we examine here is a single, steady sinusoidal mode, i.e.

$$\tilde{u}_a(x, y) = -M_U \cos(y), \tag{5.5}$$

$$\tilde{v}_a(x, y) = 0, \tag{5.6}$$

and the stream function of the flow ahead of the shock Ψ_a is

$$\Psi_a = -M_U \sin(y). \tag{5.7}$$

This velocity field is a weak shear or vorticity wave and can be considered separately from acoustic and entropy waves for weakly compressible flows (Kovásznay 1953). Turbulence is often described in terms of a large collection of sinusoidal modes of various amplitudes, wavelengths and phases. Thus, by examining the interaction of a single sinusoidal mode with a shock wave we should should gain some insight into the fundamental aspects of the shock–turbulence interaction. The sinusoidal shear flow is also the simplest periodic, non-uniform flow.

The questions addressed in this section are: When and under what conditions do kinks form (the shock focuses) in the shock front? How does the time to focus depend on $M_{S0} - 1$ and M_U? How does maximum shock strength vary with $M_{S0} - 1$ and M_U? How is shock speed affected by the interaction with a non-uniform flow? Does the shock front deform on the length scale of the energy or the enstrophy in a two-scale flow?

Initially, the shock is straight with strength $M_{S0} - 1$ and a step profile ($\partial \mu / \partial N = 0$). The simulation was run for a variety of initial strengths, $0 < M_{S0} - 1 \leqslant 0.3$, and amplitudes ahead of the shock, $0 < M_U \leqslant 0.3$.

The focusing of an acoustic discontinuity ($M_{S0} = 1$) and a weak shock wave ($M_{S0} = 1.2$) in an flow ahead of the shock with $M_U = 0.3$ are shown in figure 8(*a*) and figure 8(*b*) respectively. The evolution of shock strength for the $M_{S0} = 1$ shock is shown in figure 8(*c*). A comparison of figure 8 with figure 7 shows that the focusing mechanism is the same for a straight shock in a non-uniform flow and a curved shock in a uniform flow. In a sinusoidal flow the non-uniformity of the flow ahead of the shock bends the shock and this deformation causes the shock to strengthen in regions of concave curvature and weaken in regions of convex curvature. Eventually the shock strength breaks and shock-shocks and a shock disk form, as in the case of the initially parabolic shock. Vortex sheets and Mach stems behind the shock are associated with the kinks in the shock front (see Kevlahan 1996 for a discussion of vorticity generation behind curved shocks).
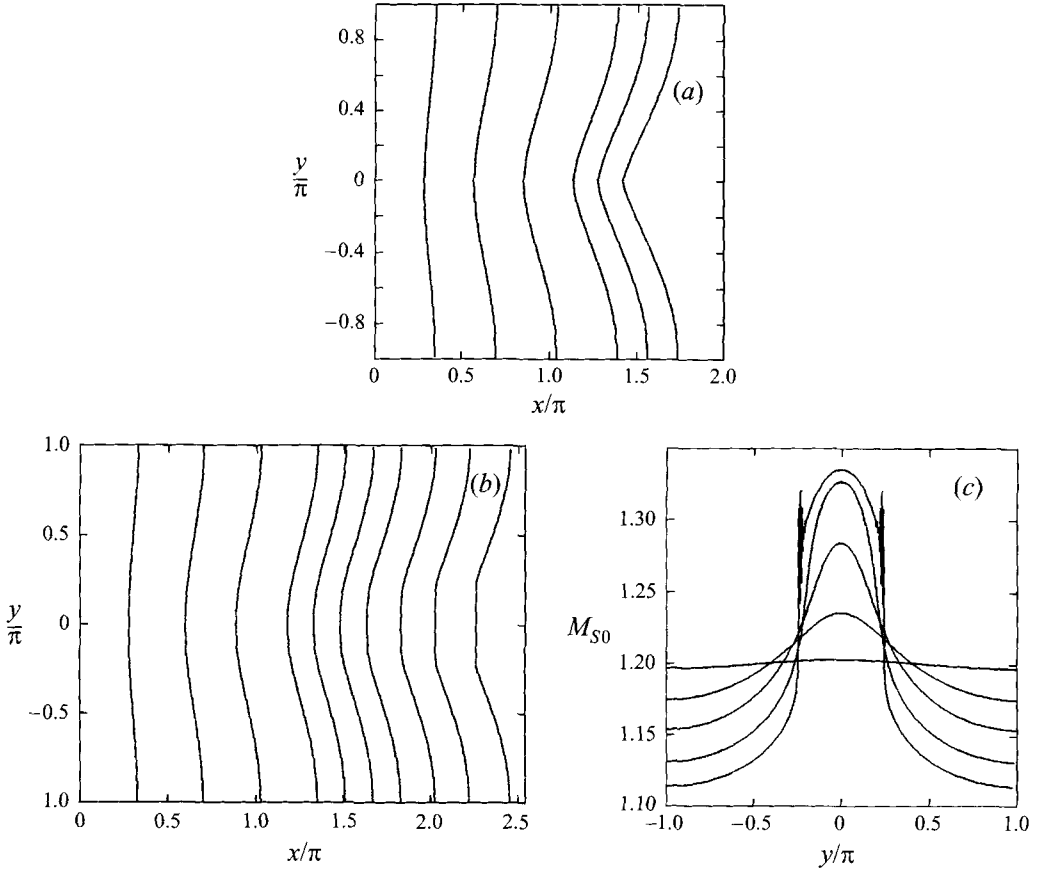
FIGURE 8. Shock focusing in a sinusoidal shear flow with $M_U = 0.1$ (times normalized by multiplying by M_{S0} for comparison purposes). (a) $M_{S0} = 1$ shock (acoustic discontinuity) at times $t = 0.99, 1.98, 2.98, 3.97, 4.46, 4.96$ (focus). (b) $M_{S0} = 1.2$ shock at times $t = 0.99, 1.98, 2.98, 3.97, 4.46, 4.96, 5.4, 6.0, 6.6, 7.3$. Note the double kinks bounding a flat shock disk. (c) Evolution of shock strength for $M_{S0} = 1.2$ shock at times $t = 0.99, 2.98, 4.46, 6.6, 7.3$. Note the appearance of shock-shocks.

The curvature at the centre of the $M_{S0} = 1$ shock wave increases like $K(0, t) = (T_C - K(0, t))^{-1}$ where the time of focus $T_C = 4.96$ for $M_U = 0.1$.

Note that the shock is sinusoidal in shape only for very short times $t < 1$, and therefore LIA (which assumes a sinusoidal distortion of the shock front) is only valid for $t \ll 1$. The LIA approximation underestimates shock deformation because it neglects shock evolution.

The dependence of time to focus $T_C M_{S0} - T_C(M_{S0} = 1)$ on initial shock strength $M_{S0} - 1$ is

$$T_C M_{S0} - 4.96 \propto (M_{S0} - 1)^{1/2}, \tag{5.8}$$

where the amplitude of the flow ahead is constant, $M_U = 0.1$.

The dependence of time to focus on the amplitude of the disturbance ahead of the shock is

$$T_C \propto (M_U - 0.03)^{-1/2}, \tag{5.9}$$

where the initial shock strength is 0.2. Thus the time to focus is an increasing function of M_U, and the shock does not focus if $M_U \leqslant 0.03$ (for $M_{S0} = 1.2$).

The dependence of the separation of the shock-shocks ΔY_C on the shock strength (for fixed $M_U = 0.1$) and on amplitude ahead of the shock (for fixed $M_{S0} - 1 = 0.2$) are given respectively by

$$\Delta Y_C \propto (M_{S0} - 1)^{-7/8}, \tag{5.10}$$

$$\Delta Y_C \propto (M_U - 0.03)^{-7/8}. \tag{5.11}$$

The maximum shock strength depends on initial shock strength and on disturbance amplitude according to the relations

$$\frac{M_{max} - 1}{M_{S0} - 1} \propto (M_{S0} - 1)^{-1/3}, \tag{5.12}$$

$$\frac{M_{max} - 1}{M_{S0} - 1} \propto M_U^{1/3}. \tag{5.13}$$

Note that ΔY_C is much larger and $(M_{max} - 1)/(M_{S0} - 1)$ is much smaller than for a parabolic shock of the same strength (for $M_U \leqslant 0.3$), although the power laws governing the dependence of ΔY_C and $(M_{max} - 1)/(M_{S0} - 1)$ on $M_{S0} - 1$ are the same.

The power-law dependencies of T_C, ΔY_C and M_{max} on $M_{S0} - 1$ are the same as those for the focusing of an initially parabolic shock. The fact that T_C and ΔY_C show the same dependence on $M_{S0} - 1$ and $1/(M_U - 0.03)$ suggests that $(M_{S0} - 1)/(M_U - 0.03)$ is a similarity parameter describing T_C and ΔY_C. Similarly, $(M_{S0} - 1)/M_U$ is a similarity parameter describing maximum shock strength at the focus.

The mean speed of the shock can be defined in several ways: e.g. from the mean advance $\langle X \rangle(t)$ of the shock in the x-direction

$$M_{Sx}(t) = 100 \left(\frac{\langle X \rangle(t)}{M_{S0} t} - 1 \right) \tag{5.14}$$

(where $M_{Sx}(t)$ is the percentage change in mean speed and the averages are normalized to take into account non-uniform spacing of grid points in the y-direction), or from the instantaneous speed of the shock in the x-direction averaged over y:

$$\frac{\mathrm{d}g(y,t)}{\mathrm{d}t} = \frac{M_S + N \cdot u_a}{N_1} = \tilde{u}_a - \frac{X_S}{Y_S} \tilde{v}_a + \frac{(X_S^2 + Y_S^2)^{1/2}}{Y_S} (1 + \tfrac{1}{4}(\gamma + 1)\mu) \tag{5.15}$$

where $x = g(y, t)$ gives the shape of the shock front. Equation (5.15) is just the SME on the level surface $G(x, y, t) = 0$ for a non-overturning shock (see equation (2.13)). To obtain the mean instantaneous shock speed $\dot{g}(t)$, $\mathrm{d}g(y, t)/\mathrm{d}t$ is averaged over all points on the shock surface (X, Y) and normalized to take into account the non-uniform spacing of the points in the y-direction.

In both the above definitions shock speed is a result of the combined effects of *velocity* magnitude ahead of the shock, *geometry* (a shock moving obliquely, $N_1 < 1$, has an increased x-displacement $\Delta g(y, t)$ even if the propagation speed M_S is unchanged), and *shock strength* (an increase in M_S leads to an increase in $\Delta g(y, t)$ even if the shock remains normal, $N_1 = 1$). The changes in geometry and shock strength are, of course, determined by the velocity field ahead of the shock and initial shock shape. Note that M_S is constant for an acoustic shock, and therefore any changes in shock speed can only come from geometrical effects.

The percentage change in $\dot{g}(t)$ as a function of time for various shock strengths with $M_U = 0.1$ is shown in figure 9(a), and a similar graph for varying M_U with fixed $M_{S0} - 1 = 0.2$ is shown in figure 9(b); the equivalent graphs for $M_{Sx}(t)$ are shown in figures 10(a) and 10(b). It is found that $M_{Sx}(t) \propto t^2$ for $M_{S0} = 1$, and for $t < 4$
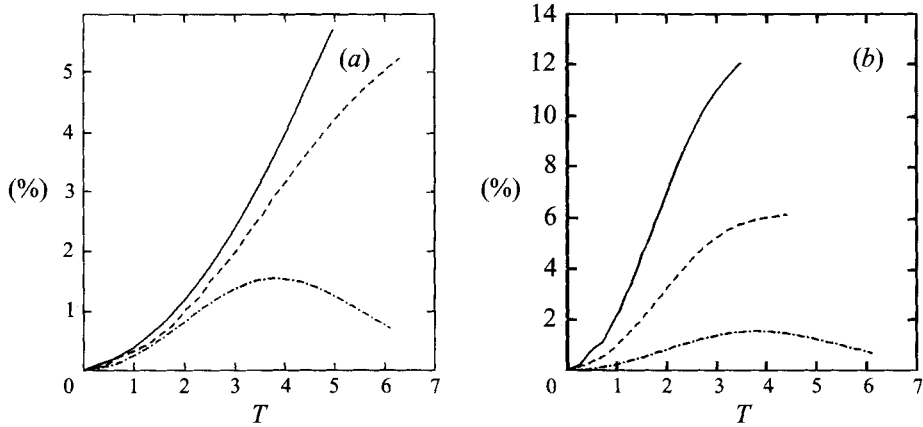
FIGURE 9. Percentage increase in instantaneous mean shock speed in the x-direction as a function of time. (a) Fixed disturbance amplitude ahead of the shock $M_U = 0.1$, shock strengths $M_{S0} - 1 = 0$ (—), 0.05 (- - -), 0.2 (— · —). (b) Fixed initial strength $M_{S0} = 1.2$, disturbance amplitude $M_U = 0.3$ (—), 0.2 (- - -), 0.1 (— · —).
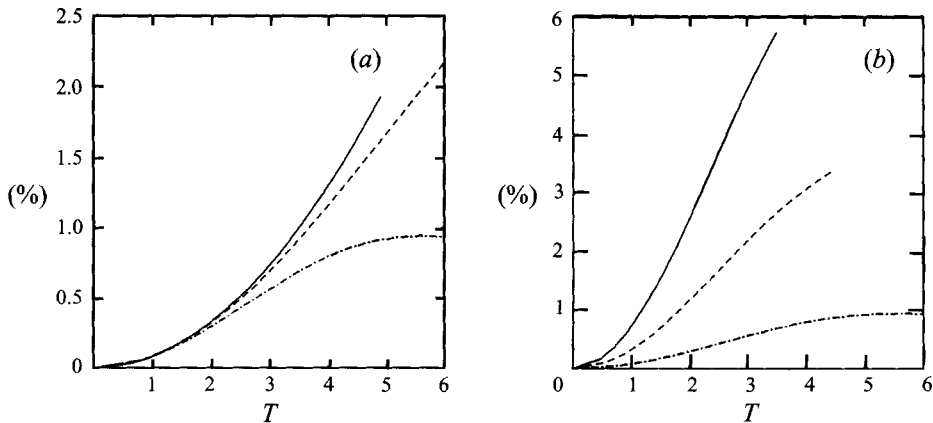

FIGURE 10. Percentage increase in mean shock speed based on mean advance in the x-direction as a function of time. (a) Fixed disturbance amplitude ahead of the shock $M_U = 0.1$, shock strengths $M_{S0} - 1 = 0$ (—), 0.05 (- - -), 0.2 (— · —). The mean speed for $M_{S0} - 1 = 0$ increases like t^2. (b) Fixed initial strength $M_{S0} = 1.2$, disturbance amplitude $M_U = 0.3$ (—), 0.2 (- - -), 0.1 (— · —).

if $M_{S0} > 1$. For $t > 4$ the increase in speed is slower. The increase in instantaneous speed is slightly slower (but qualitatively the same) compared to speed based on mean advance of the shock, e.g. $\dot{g} \propto t^{1.7}$ for $M_{S0} = 1$.

An example of instantaneous shock speed at a focus as a function of y is shown in figure 11(a), and an example of shock position at a focus compared with the position of the equivalent plane shock in uniform flow shock is shown in figure 11(b). The acoustic shock shows a large change in instantaneous shock speed because of its single-kink geometry and the fact that shock strength remains constant. The $M_{S0} = 1.2$ shock, unlike the acoustic shock, shows an increase in speed around $y = 0$ (where, in this case, the geometrical effect is zero) as well as around $y = \pm 1$. The variation in shock strength causes the $M_{S0} = 1.2$ shock to become much flatter than the acoustic shock, and thus reduces the geometrical effect. The net effect of variation
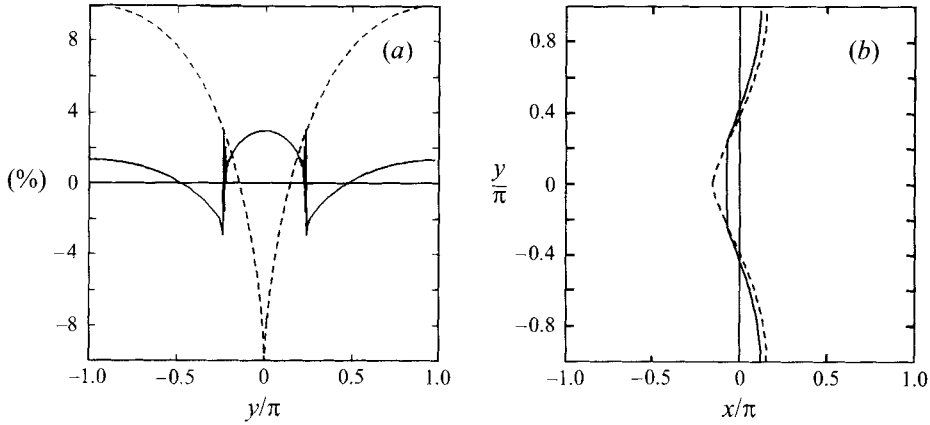
FIGURE 11. (a) Percentage change in the instantaneous mean shock speed in the x-direction as a function of y for $M_{S0} - 1 = 0.2$ (——) and $M_{S0} - 1 = 0$ (- - -); $M_U = 0.1$, $T = T_C$). (b) Shock position (——) compared with the position of an acoustic discontinuity at the focus (- - -) and the position of an equivalent plane shock in uniform flow (same parameters as a).

in shock strength is seen to be a smaller increase in shock speed compared with the acoustic shock (where changes in shock speed are due entirely to geometric effects).

The shock always travels faster in the non-uniform flows than in a uniform flow, the maximum increase being 12% (this would correspond to an increase of 48 m s^{-1} for a shock travelling near the speed of sound in air) for $M_{S0} - 1 = 0.2$ and $M_U = 0.3$. This increase in speed is due to the dynamical evolution of the shock, both in shape and in strength.

A turbulent flow contains motion on a wide range of length scales. The motion at the largest scales has most of the energy, but the motion at the smaller scales has most of the enstrophy (i.e. there are strong gradients in the velocity at small scales). When a shock passes through a turbulent flow does it distort on the large length scales (energetic) or on the small length scales (vortical)? To answer this question in the case of a typical uni-directional flow ahead of the shock we now look at a shock propagating through the following velocity field:

$$\tilde{u}_a(x, y) = -M_U(\cos(y) + 10^{-5/6} \cos(10y)), \tag{5.16}$$

$$\tilde{v}_a(x, y) = 0, \tag{5.17}$$

where the factor $10^{-5/6}$ comes from assuming a Kolmogorov $k^{-5/3}$ energy spectrum.

The shape of the shock in the two-scale velocity field at the focus is shown in figure 12(a) and its strength is shown in figure 12(b). The overall shape of the shock is clearly determined by the energetic length scale, but kinks in the shock front form at the minima of the vortical length scale. These 'vortical' kinks form before the 'energetic' kinks ($T_C = 2.4$ compared with $T_C = 5.8$). This two-scale calculation is repeated for a two-dimensional flow ahead of the shock in the following section.

5.3. *Vortex array*

In the previous section we examined shock propagation into a one-dimensional sinusoidal flow, we now investigate for the first time a weak shock propagating into a velocity field with sinusoidal modes in two perpendicular directions (a *vortex array*). The flow ahead is specified by the stream function

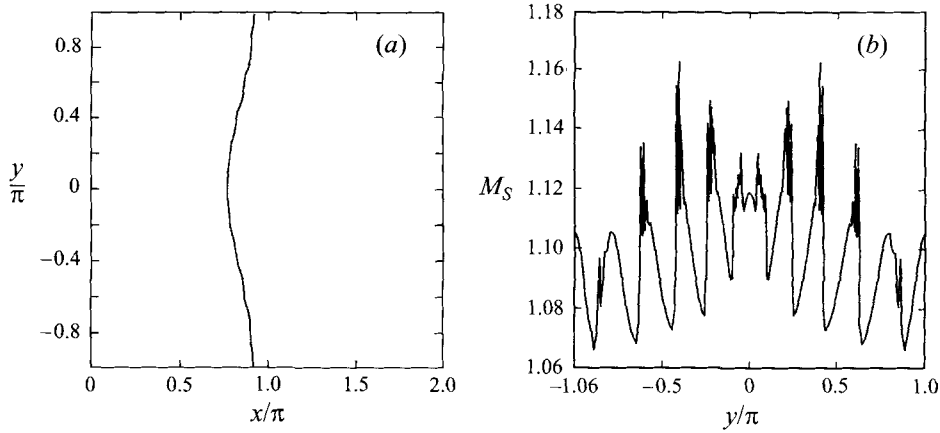$$\Psi_a(x, y) = -M_U \cos(x) \sin(y), \tag{5.18}$$

FIGURE 12. Shock focusing in a two-scale velocity field ($M_{S0} - 1 = 0.1$, $M_U = 0.1$, $T = T_C = 2.4$). (a) Shock shape. Note that the overall deformation is on the large length scale (energetic), but that kinks have formed on the small length scale (vortical). (b) Shock strength. Note the peaks due to minima in the small-scale vortical part of the velocity field.

which has the corresponding velocity field

$$\tilde{u}_a(x, y) = -M_U \cos(x) \cos(y),\qquad(5.19)$$

$$\tilde{v}_a(x, y) = -M_U \sin(x) \sin(y),\qquad(5.20)$$

and vorticity field

$$\omega_a(x, y) = -2M_U \cos(x) \sin(y).\qquad(5.21)$$

The flow specified by the stream function (5.18) is an infinite array of two-dimensional vortices of alternating sign with centres at $x = \pi(n - 1)$, $y = \pi/2(2n - 1)$.

As in the case of the uni-directional sinusoidal shear flow, kinks form in the shock front due to focusing. However, in this case the conditions under which kinks form is more restrictive. We examined shocks starting from $x = 0$ (where the flow enhances focusing) and starting from $x = \pi/2$ (where the flow inhibits focusing). Kinks form for all $M_{S0} - 1$ and for $M_U > 0.10$ in the case $x_0 = 0$ and for $M_{S0} - 1 < 1.15$ and for $M_U > 0.05$ in the case $x_0 = \pi/2$.

Figure 13 shows a comparison of the focusing of an acoustic discontinuity $M_{S0} = 1$ and of a moderately weak shock $M_{S0} = 1.2$ for a large disturbance amplitude $M_U = 0.3$. Note that the convergence region at $(\pi/2, 0)$ enhances focusing, and that later the convergence region at $(3\pi/2, 0)$ pulls the kinks apart. The time to focus is much quicker than in the uni-directional case, $T_C = 2.6$ compared with $T_C = 4.1$.

Time to focus and maximum shock strength at the focus in the case $x_0 = 0$ vary according to

$$(T_C M_{S0} - 9.3) \propto (M_{S0} - 1)^{1/2}, \quad M_{S0} < 1.1,\qquad(5.22)$$

$$\frac{M_{max} - 1}{M_{S0} - 1} \propto (M_{S0} - 1)^{-1/3},\qquad(5.23)$$

where $T_C = 9.3$ for an acoustic discontinuity. There is not a large enough range to establish power laws for the variable-M_U case.

If the shock is started at $x_0 = \pi/2$ then

$$(T_C M_{S0} - 5.6) \propto (M_{S0} - 1)^{2/3},\qquad(5.24)$$

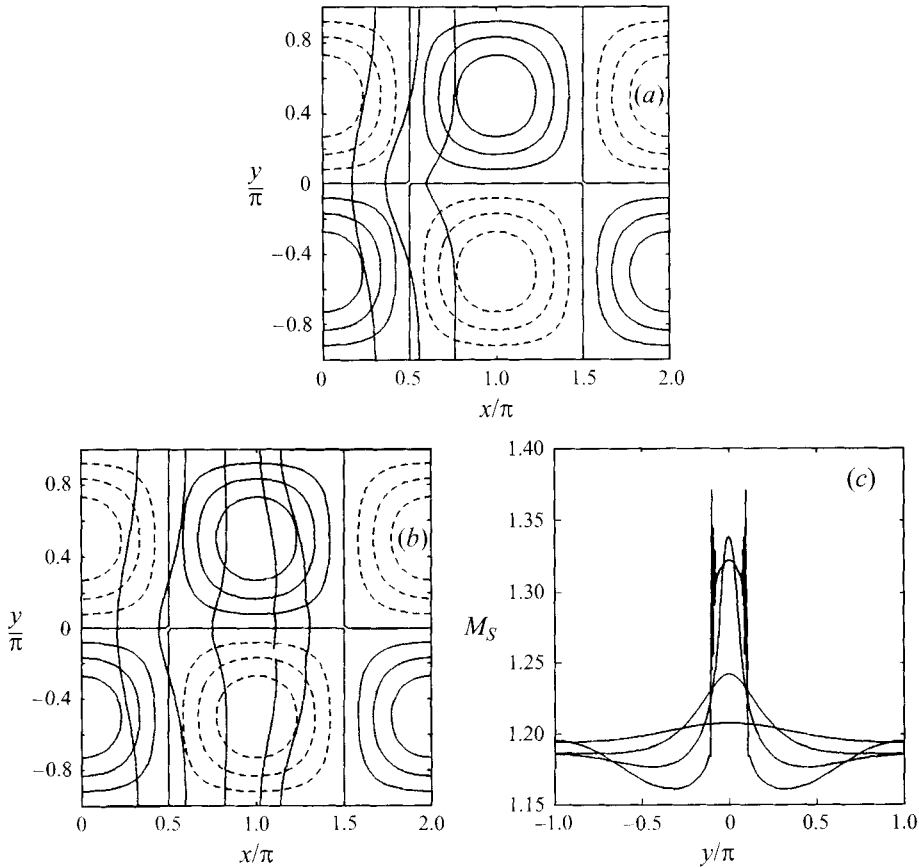$$T_C \propto (M_U - 0.05)^{-0.6},\qquad(5.25)$$

FIGURE 13. Shock focusing in a two-dimensional vortex array with disturbance amplitude $M_U = 0.3$. (a) Acoustic discontinuity $M_{S0} = 1$ at times $t = 0.75$, 1.50, 2.25 (left to right). (b) Moderately weak shock $M_{S0} = 1.2$ at times $M_{S0}t = 0.84$, 1.68, 2.52, 3.36, 3.84. (c) Variation of shock strength for $M_{S0} = 1.2$ shock at times $M_{S0}t = 0.84$, 1.68, 2.52, 3.36. Note how the flow pulls the kinks apart.

$$\frac{M_{max} - 1}{M_{S0} - 1} \propto (M_{S0} - 1)^{-1/3}, \tag{5.26}$$

$$\frac{M_{max} - 1}{M_{S0} - 1} \propto M_U^1, \quad M_U > 0.15, \tag{5.27}$$

where $T_C = 5.6$ for an acoustic discontinuity.

The change in propagation speed of the shock for various strengths as a function of time is shown in figure 14(a), and for various M_U in figure 14(b). Again, except for very long times (several eddy diameters), the shock moves faster in the vortex array than in uniform flow in all cases. The greatest increase is roughly 1.5% for $M_U = 0.3$ and $M_{S0} = 1.2$. This increase in propagation speed is achieved in the length scale of a single eddy. Note that the increase in speed is less than in the case of the unidirectional sinusoidal shear flow.

As in the previous section, the shock was also propagated through a two-scale velocity field to determine whether the shock deforms on the small (vortical) length scale, or the large (energetic) length scale. The two-scale velocity field had the stream function

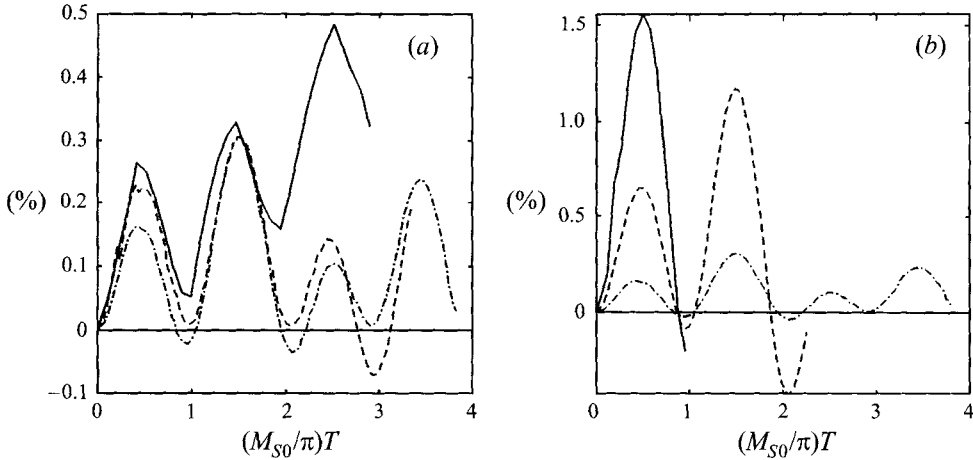$$\Psi_a(x, y) = -M_U(\cos(x)\sin(y) + 10^{-5/6}\cos(10x)\sin(10y)). \tag{5.28}$$

FIGURE 14. Instantaneous mean shock speed in the x-direction as a function of time ($x_0 = \pi/2$). (a) Fixed disturbance amplitude ahead of the shock $M_U = 0.1$, shock strengths $M_{S0} - 1 = 0$ (—), 0.05 (- - -), 0.2 (— · —). (b) Fixed initial strength $M_{S0} = 1.2$, disturbance amplitude $M_U = 0.3$ (—), 0.2 (- - -), 0.1 (— · —).

It was found that there is essentially no difference between the shock shape in the single- and two-scale velocity fields. Unlike the uni-directional case, kinks do not form at the minima of the small-scale field. This result suggests that in real turbulence the shock deformation is determined essentially by the energy-containing scales of motion; the smaller vortical scales have little effect. DNS simulations confirm this conclusion, showing no small wiggles on the shock front (see figure 4 in Kevlahan *et al.* 1992).

In turbulence where the average correlation length of the flow is approximately one eddy long a shock is unlikely to focus unless kinks form within a single eddy. From the results obtained here, a rough guide is that shock focusing will occur in turbulence if $M_{S0}/M_U < 4$–7 where we have used the fact that turbulence Mach number, M_t, is the average Mach number of the flow. For example, an $M_S = 1.2$ shock focuses in turbulent flows with $M_t > 0.17$–0.30 (where M_S is the Mach number of the laminar shock).

5.4. Point-vortex array

We now investigate for the first time how a weak shock wave interacts with a singular flow: a one dimensional array of point vortices. These vortices have a structure that is similar to the vortices in a turbulent flow.

The velocity field of a row of point vortices of strength κ at $y = mb$ and $-\kappa$ at $y = (m + \frac{1}{2})b$ may be found using the method of Saffman (1992, pp. 133–138):

$$\tilde{u}_a(x, y) = \frac{\kappa}{b} \frac{\sin\left((2\pi/b)y\right)\cosh\left((2\pi/b)x\right)}{\cosh^2\left((2\pi/b)x\right) - \cos^2\left((2\pi/b)y\right)}, \tag{5.29}$$

$$\tilde{v}_a(x, y) = -\frac{\kappa}{b} \frac{\cos\left((2\pi/b)y\right)\sinh\left((2\pi/b)x\right)}{\cosh^2\left((2\pi/b)x\right) - \cos^2\left((2\pi/b)y\right)}. \tag{5.30}$$

Near the origin the point-vortex velocities become

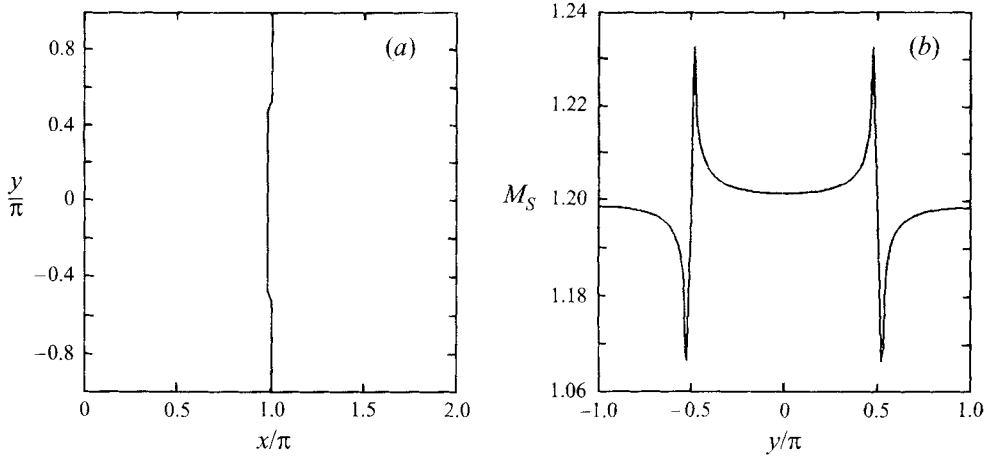$$u(x, y)_a = \frac{\kappa}{2\pi} \frac{y}{x^2 + y^2}, \tag{5.31}$$

FIGURE 15. Shock focusing in a Rankine vortex array, $M_{S0} = 1.2$, $M_U = 0.3$. (a) Shock shape at the focus (point-vortex array at $y = 0$). Note kinks at $y = \pm\pi/2$, the locations of the vortices. (b) Shock strength at the focus. Note the large decrease in shock strength on the positive velocity side of the vortices.

$$v(x, y)_a = -\frac{\kappa}{2\pi}\frac{x}{x^2 + y^2}, \qquad (5.32)$$

which is just the velocity field for a point vortex. For large distances x from the array the velocity field becomes

$$\tilde{u}_a(x, y) = \frac{2\kappa}{b}\sin\left((2\pi/b)y\right)e^{-(2\pi/b)x}, \qquad (5.33)$$

$$\tilde{v}_a(x, y) = -\frac{2\kappa}{b}\cos\left((2\pi/b)y\right)e^{-(2\pi/b)x}, \qquad (5.34)$$

i.e. the velocity field decreases exponentially away from the vortex array.

In order to avoid the singularity at the centre of the vortex the point vortices are given solid-body-rotation cores, producing a Rankine vortex. Note that because we are interested in the effect of the singular velocity profile of the flow we deliberately do not use a vortex with a smooth (e.g. Gaussian) distribution of vorticity. Matching the velocity at the core boundary gives the velocity field of the core:

$$u_{core}(x, y) = \frac{\kappa}{2\pi r_0^2}y, \qquad (5.35)$$

$$v_{core}(x, y) = -\frac{\kappa}{2\pi r_0^2}x, \qquad (5.36)$$

where r_0 is the radius of the vortex core.

In the simulation $-\pi < y < \pi$ (y is shifted by $y = -\pi/2$), $b = 2\pi$, $r_0 = 0.10$, and $\kappa = M_U/2\pi$ (which gives a maximum speed of M_U at the core boundary). Figures 15(a) and 15(b) show the shock shape and strength at the time kinks form. Kinks form as soon as the shock reaches the core, and move together as the shock propagates.

The shock focusing observed here is different in two important ways from shock focusing in the non-singular flows considered earlier. First, all values of shock strength and M_U lead to the formation of kinks; even M_U as small as 0.0001 causes the shock to focus. Secondly, T_C and M_{max} vary only slightly with M_t, and M_{max} is only about 3% greater than M_{S0}. These results indicate that it is the singular $1/r$ form of the

velocity field that turns the shock and produce kinks; its magnitude is not important. Again, remember that the solid-body-rotation core removes the actual point vortex singularity.

If the eddies of turbulence have a $1/r$ velocity fall-off these results suggest that kinks may form at much lower values of M_t than were estimated based on the results of the vortex array simulation. Vortex sheets will form behind the kinks and thus one might expect significant enstrophy production in the shock–turbulence interaction, even for relatively small values of M_t.

6. Conclusions

In this paper we have reviewed the current approaches for treating the propagation of weak shocks in uniform and non-uniform flows. We noted that current weak shock theory fails near a focus and is unsuitable for non-uniform flows ahead of the shock, and that non-DNS treatments of the shock–turbulence interaction do not take into account shock evolution.

The novel shock manifold/compatibility condition method of Ravindran & Prasad (1993) is used to describe shock propagation. This method is extended here to non-uniform flows ahead of the shock and the infinite set of compatibility conditions is closed by making the weak shock assumption, i.e. that the normalized density jump is small, $\mu \ll 1$. We derived a set of equations (2.43), (2.49), (2.13) describing the propagation of a weak shock discontinuity into two-dimensional non-uniform flow in motion. These equations were derived rigorously as an $O(\mu)$ approximation from the equations of gasdynamics and the Rankine–Hugoniot jump conditions. The acoustic approximation was used for the flow ahead (i.e. products of fluctuating quantities ahead of the shock are neglected) and thus the shock equations are valid in the range $M_U^2 \leqslant \mu \ll 1$, where M_U is the Mach number of the flow ahead. No models were used.

If the magnitude of the terms ahead of the shock is less than $O(\mu)$ (i.e. $M_U < \mu$) then the terms ahead of the shock in the compatibility equations (2.43) and (2.49) may be neglected and the shock propagation equations become simply

$$\frac{\mathrm{d}X}{\mathrm{d}t} = N_1 \left[1 + \tfrac{1}{4}(\gamma + 1)\mu\right] + \tilde{u}_a, \quad \frac{\mathrm{d}Y}{\mathrm{d}t} = N_2 \left[1 + \tfrac{1}{4}(\gamma + 1)\mu\right] + \tilde{v}_a,$$

$$\frac{\mathrm{d}\mu}{\mathrm{d}t} = \frac{1}{2} \left[\frac{\partial\theta}{\partial S} - \tfrac{1}{2}(\gamma + 1)\frac{\partial\mu}{\partial N}\right]\mu, \quad \frac{\mathrm{d}}{\mathrm{d}t}\left(\frac{\partial\mu}{\partial N}\right) = \frac{1}{2}\left[\frac{\partial\theta}{\partial S} - (\gamma + 1)\frac{\partial\mu}{\partial N}\right]\frac{\partial\mu}{\partial N}.$$

The shock equations cannot be solved exactly, except in a few simple situations, and thus a numerical method of solution was developed. The numerical method uses an adaptive non-uniform grid in which the resolution changes over time such that regions of high shock strength (large concave curvature) are resolved more finely than regions of low shock strength. This method is particularly suited to examining the behaviour of a shock near a focus (where the strength increases).

An $O(\mu^2)$ version of the shock equations was also derived in order to check that no qualitatively new effects arise by including higher-order terms.

The shock equations were verified analytically against known solutions for the propagation of a plane N-wave weak shock and an expanding cylindrical weak shock. The Guderley self-similarity solution for converging strong shocks was also determined to within 13.5% as the limit of the solutions of the second-order shock equations. The numerical solution of the shock equations was also checked against a full DNS for the case of an initially plane shock propagating into a sinusoidal

Case	$T_C M_{S0} - T_C(M_{S0} = 1)$	ΔY_C	$(M_{max} - 1)/(M_{S0} - 1)$
parabola	$1/2$	$7/8$	$-1/3$
shear	$1/2$	$7/8$	$-1/3$
array	$1/2$ $2/3$	—	$-1/3$

TABLE 1. The dependence on shock strength $(M_{S0} - 1)^n$. The amplitude of the flow ahead of the shock was constant $M_U = 0.1$ for the sinusoidal shear and vortex array cases.

Case	$T_C M_{S0} - T_C(M_{S0} = 1)$	ΔY_C	$(M_{max} - 1)/(M_{S0} - 1)$
shear	$(M_U - 0.03)^{-1.2}$	$(M_U - 0.03)^{-7/8}$	$M_U^{1/3}$
array	$(M_U - 0.05)^{-0.6}$	—	$M_U^{1/3}$

TABLE 2. The dependence on velocity amplitude ahead of the shock M_U^n. The initial strength of the shock was fixed $(M_{S0} - 1) = 0.2$.

shear flow. The DNS resolved the internal structure of the shock and solved the full Navier–Stokes equations. The agreement was excellent (the error was less than the shock width), even at the time of focus when shock-shocks develop. A way of extending the shock propagation equations solution past the time of focus by propagating the shock disk and wings separately was also verified against DNS.

The fact that the shock equations (which assume that the shock is discontinuous) agree so well with DNS which actually resolves the shock structure indicates that one may safely neglect shock thickness, even in the case of curved shocks. This result contradicts Germain & Guiraud (1966)'s assertion that shock thickness must be included in a description of the propagation of curved shocks.

The shock equations were applied to the problem of the focusing of an initially parabolic shock. The resulting shock shapes agreed well with the experimental results of Sturtevant & Kulkarny (1976). Focusing also occurred in the case of a shock propagating into a sinusoidal shear flow, a vortex array (perpendicular sinusoidal modes) and a linear array of point vortices. The results on the time to focus T_C, separation of shock-shocks ΔY_C and maximum strength at the focus M_{max} are summarized in tables 1 and 2. These results show that the focusing of an initially parabolic shock and an initially straight shock in sinusoidal shear flow (and, more generally, any unidirectional flow with a minimum in the velocity) is essentially the same process. The dependence of T_C and M_{max} on initial shock strength is very similar for all the flows; the relations $(M_{max} - 1)/(M_{S0} - 1) \propto (M_{S0} - 1)^{-1/3}$ and $T_C M_{S0} - T_C(M_{S0} = 1) \propto (M_{S0} - 1)^{-1/2}$ appear to be very general. The results for the dependence of shock focusing on M_U indicate that no focusing occurs for $M_U < 0.03$–0.05.

Tables 1 and 2 show that T_C and ΔY_C have the same dependence on $M_{S0} - 1$ and $1/(M_U - 0.03)$. This suggests that $(M_{S0} - 1)/(M_U - 0.03)$ is a similarity parameter describing T_C and ΔY_C. Similarly, $(M_{S0} - 1)/M_U$ is a similarity parameter describing maximum shock strength at the focus.

The vortex array results can be used to provide a rough estimate of the conditions under which a shock may focus in turbulence. Focusing may occur in turbulence if $M_t/M_S > 0.14$–0.25, where M_t is the average Mach number of the turbulence and M_S is the Mach number of the shock in a flow at rest.

The average propagation speed of a shock in a two-dimensional vortex array may

be up to 1.5% faster than the propagation speed of the same shock in non-uniform flow at rest. This increase in propagation speed is achieved in the length scale of a single eddy. The shock always moves faster in a non-uniform flow (except for very long times). The change in propagation speed is the result of a combination of changes in shock geometry and shock strength. The geometrical effects are larger and decrease as initial shock strength increases. These results agree qualitatively with those of Lee *et al.* (1993) who found a 0.7% forward drift speed for a weak shock interacting with incompressible turbulence. Lele (1992) estimated analytically a 0.4% increase in shock speed, but neglected the evolution of the shock front. It is likely that the remainder of the increase in shock speed is caused the evolution of the shock.

Using two-scale velocity fields it was determined that the shock deforms on the (larger) length scale of the energy. Kinks form on the (smaller) length scale of the enstrophy in the sinusoidal shear flow, but kinks do not form at the small length scale in the two-dimensional vortex array.

To examine the effect of a singular velocity field on shock propagation a flow ahead of the shock consisting of a linear array of point vortices with solid-body-rotation cores was considered. It was found that kinks formed at even the smallest values of M_U, but that $M_{max} - M_{S0}$ was small.

In summary, we have derived a new set of equations describing the propagation of a curved weak shock in subsonic non-uniform flows. These equations have been verified against known analytical solutions and against a full direct numerical simulation. The focusing of shocks in uniform and non-uniform flows has been investigated and some general relations have been deduced. In particular, it has been found that a shock in a two-dimensional vortex array moves up to 1.5% faster than the same shock in a uniform flow at rest.

REFERENCES

ANYIWO, J. C. & BUSHNELL, D. M. 1982 Turbulence amplification in shock-wave and boundary-layer interaction. *AIAA J.* **20**, 893–899.

BRYSON, A. E. & GROSS, R. W. F. 1961 Diffraction of strong shocks by cones, cylinders and spheres. *J. Fluid Mech.* **10**, 1–16.

CATHERASOO, C. J. & STURTEVANT, B. 1983 Shock dynamics in non-uniform media. *J. Fluid Mech.* **127**, 539–561.

COURANT, R. & FRIEDRICHS, K. O. 1948 *Supersonic Flow and Shock Waves.* Interscience Publishers.

COURANT, R. & HILBERT, D. 1953 *Methods of Mathematical Physics.* Interscience.

DURBIN, P. A. & ZEMAN, O. 1992 Rapid distortion theory for homogeneous turbulence with application to modelling. *J. Fluid Mech.* **242**, 349–370.

GERMAIN, P. & GUIRAUD, J.-P. 1966 Conditions de choc et structure des ondes de choc dans un écoulement non stationnaire de fluide dissipatif. *J. Math. Pures Appl.* **45**, 311–358.

GRINFEL'D, I. M. 1978 Ray method for calculating the wavefront intensity in nonlinear elastic material. *J. Appl. Math. Mech.* **42**, 958–977.

GUDERLEY, G. 1942 Starke kugelige und zylindrische Verdichtungsstösse in der Nähe des Kugelmittelpunktes bzw der Zylinderachse. *Luftfahrtforschung* **19**, 302–312.

HAYES, W. D. 1968 Self-similar strong shocks in an exponential medium. *J. Fluid Mech.* **32**, 305–315.

HUNT, J. C. R. & VASSILICOS, J. C. 1991 Kolmogorov's contribution to the physical and geometrical understanding of small-scale turbulence and recent developments. *Proc. R. Soc. Lond.* A**434**, 183–210.

KELLER, J. B. 1954 Geometrical acoustics. I. The theory of weak shock waves. *J. Appl. Phys.* **25**, 938–947.

KEVLAHAN, N. 1996 The vorticity jump across a shock. Submitted to *J. Fluid Mech.*

KEVLAHAN, N., KRISHNAN, M. & LEE, S. 1992 Evolution of the shock front and turbulence structures in the shock/turbulence interaction. In *Studying Turbulence using Numerical Simulation Databases - IV, Proc. 1992 Summer Program.* Stanford: CTR.

KIDA, S. & ORSZAG, S. A. 1990 Enstrophy budget in decaying compressible turbulence. *J. Sci. Comput.* **5**, 1–34.

KOVÁSZNAY, L. S. G. 1953 Turbulence in supersonic flow. *J. Aero. Sci.* **20**(10), 657–682.

KULKARNY, V. A. & WHITE, B. S. 1982 Focusing of waves in a turbulent inhomogeneous media. *Phys. Fluids* **25**, 1770–1784.

LANDAU, L. D. 1945 On shock waves at large distances from the place of their origin. *Sov. J. Phys.* **9**, 496–500.

LEE, S., LELE, S. K. & MOIN, P. 1993 Direct numerical simulation of isotropic turbulence interacting with a weak shock wave. *J. Fluid Mech.* **251**, 533–562.

LELE, S. K. 1992 Shock-jump relations in a turbulent flow. *Phys. Fluids* A **4**, 2900–2905.

MCKENZIE, J. F. & WESTPHAL, K. O. 1968 Interaction of linear waves with oblique shock waves. *Phys. Fluids* **11**, 2350–2362.

MASLOV, V. P. 1978 Propagation of shock waves in an isentropic non-viscous gas. *J. Sov. Math.* **13**; English transl. (1980) 119–163.

MOORE, F. K. 1953 Unsteady oblique interaction of a shock wave with a plane disturbance. *NACA TN-2879.*

OBERMEIER, F. 1983 On the propagation of weak and moderately strong, curved shock waves. *J. Fluid Mech.* **129**, 123–136.

PETERS, N. 1992 A spectral closure for premixed turbulent combustion in the flamelet regime. *J. Fluid Mech.* **242**, 611–629.

PRASAD, P. 1982 Kinematics of a multi-dimensional shock of arbitrary strength in an ideal gas. *Acta Mech.* **45**, 163–176.

PRASAD, P., RAVINDRAN, R. & SAU, A. 1991 The characteristic rule for shocks. *Appl. Math. Lett.* **4**, 5–8.

RAVINDRAN, R. & PRASAD, P. 1993 On an infinite system of compatibility conditions along a shock ray. *Q. J. Mech. Appl. Maths*, **46**, 131–140.

RAVINDRAN, R., SUDER, S. & PRASAD, P. 1994 Long time behaviour of the solution of a system of equations from new theory of shock dynamics. *Comput. Math. Appl.* **27**(12), 91–104.

RIBNER, H. S. 1954 Convection of a pattern of vorticity through a shock wave. *NACA TN-2864.*

SAFFMAN, P. G. 1992 *Vortex Dynamics.* Cambridge University Press.

STURTEVANT, B. & KULKARNY, V. A. 1976 The focusing of weak shock waves. *J. Fluid Mech.* **73**, 651–671.

VAN DYKE, M. & GUTTMANN, A. J. 1982 The converging shock wave from a spherical or cylindrical piston. *J. Fluid Mech.* **120**, 451–462

VASSILICOS, J. C. & HUNT, J. C. R. 1992 Turbulent flamelet propagation. *Combust. Sci. Tech.* **87**, 291–327.

WHITHAM, G. B. 1957 A new approach to problems of shock dynamics. Part I. Two-dimensional problems. *J. Fluid Mech.* **2**, 145–171.

WHITHAM, G. B. 1968 A note on shock dynamics relative to a moving frame. *J. Fluid Mech.* **31**, 449–453.

WHITHAM, G. B. 1974 *Linear and Nonlinear Waves.* John Wiley & Sons.

WILLIAMS, F. A. 1985 Turbulent combustion. In *The Mathematics of Combustion* (ed. J. Buckmaster), pp. 97–131. SIAM.